ÅBO AKADEMI

MATEMATISK-
NATURVETENSKAPLIGA
FAKULTETEN

FACULTY OF MATHEMATICS
AND NATURAL SCIENCES

Processkemiska centret

Process Chemistry Centre

REPORT 08-07

Crystallization Characteristics of Bioactive Glasses

Hanna Arstila

Process Chemistry Centre
Laboratory of Inorganic Chemistry
2008

Supervisors

Docent Leena Hupa
Laboratory of Inorganic Chemistry
Process Chemistry Centre
Åbo Akademi University
Åbo, Finland

and

Professor Mikko Hupa
Laboratory of Inorganic Chemistry
Process Chemistry Centre
Åbo Akademi University
Åbo, Finland

Reviewer

Docent Heidi Fagerholm
Ahlstrom Glassfibre Oy
Kotka, Finland

Reviewer and Opponent

Professor Yuanzheng Yue
University of Aalborg
Aalborg, Denmark

ISSN 1459-8205
ISBN 978-952-12-2161-3
UNIPRINT
Åbo, Finland, 2008

PREFACE

This work was carried out at the Process Chemistry Centre at Åbo Akademi University during the years 2003-2008. Funding for the doctoral activities was provided by the ComBio Technology Programme run by the Finnish Funding Agency of Technology and Innovation, Tekes. Vivoxid Ltd, Linvatec Biomaterials Ltd, Bioretec Ltd and BBS are also acknowledged for their support. This work was part of the activities of the National Biomaterial and Tissue Engineering Graduate School.

I am deeply grateful to my primary supervisor Docent Leena Hupa for being so patient yet encouraging. This thesis would look a lot different without your enormous help which I am humbly thankful for. I admire your knowledge of glass science and your ability to "crystallize" thoughts to paper. I am very proud for having you as my supervisor.

I would also like to express my gratitude to Professor Mikko Hupa for giving me the opportunity to be a part of the Process Chemistry Centre. I highly appreciate your support during the Biowaffle project. I will further thank my external supervisor Professor Hannu Aro for supporting my Biomaterial Graduate School activities.

A special thanks goes to Docent Heimo Ylänen for giving me the opportunity to work with bioactive glasses already at 1999. A part-time work with glass melting, sintering and SBF-tests led to master thesis and finally to Biowaffle project and this thesis. I consider myself privileged for working with such interesting issues and with so broad range of experts. I would like to thank all the members of the Biowaffle group for their contribution to this work, especially my co-authors Mr. Mikko Tukiainen, Professor Minna Kellomäki and Mrs. Jessica Alm. Dr. Fredrik Ollila and Dr. Ilkka Kangasniemi from Vivoxid are also acknowledged for sharing interest to fiber production related issues.

I have been so lucky to have such great colleagues. I would like to thank the whole CMC group for all the great moments, honestly. I will miss you all, but especially you Linda and Erik. You have given me not only years of good collaboration, but also a life long friendship. I would also like to thank you Di, Minna and Suski for good collaboration and travel companion. A special thanks go to Jaana; I am in depth to you for your help in the lab. I will remember the hours we have spent by the furnace waiting for the glass fibers to drop. I would also like to thank Micki for helping with numerous technical things like building the fiber drawing system, Fröbbe for also helping me with technical things and Clifford and Linus for SEM analysis. Mrs. Pia Sundberg and Mrs. Katri Lindholm deserve thanks for sharing data from their Master thesis.

Finally, I would like to thank all my friends and family for your support. Without the help and patience of my parents, my mother- and father-in-law and nanny Alli for taking care of Klaus, this thesis would not have been written yet. Kaapo, thank you for being there for me, always.

Åbo, September 2008

Hanna Arstila

ABSTRACT

Bioactive glasses are excellent candidates for implant materials, because they can form a chemical bond to bone or guide bone growth, depending on the glass composition. Some compositions have even shown soft tissue attachment and antimicrobial effects. So far, most clinical applications are based on monoliths, plates and particulates of different grain sizes. There is a growing interest in special products such as porous implants sintered from microspheres and fibers drawn from preforms or glass melts. The viscosity range at which these are formed coincides with the crystallization temperature range for most bioactive glasses, thus complicating the manufacturing process.

In this work, the crystallization tendency and its kinetics for a series of glasses with their compositions within the range of bioactivity were investigated. The factors affecting crystallization and how it is related to composition were studied by means of thermal analysis and hot stage microscopy. The crystal compositions formed during isothermal and non-isothermal heat treatments were analyzed with SEM-EDXA and X-ray diffraction analysis. The temperatures at which sintering and fiber drawing can take place without interfering with crystallization were determined and glass compositions which are suitable for these purposes were established. The bioactivity of glass fibers and partly crystallized glass plates was studied by soaking them in simulated body fluid (SBF). The thickness of silica, calcium and phosphate rich reaction layers on the glass surface after soaking was used as an indication of the bioactivity.

The results indicated that the crystallization tendencies of the experimental glasses are strongly dependent on composition. The main factor affecting the crystallization was found to be the alkali oxide content: the higher the alkali oxide content the lower the crystallization temperature. The primary crystalline phase formed at low temperatures in these glasses was sodium calcium silicate. The crystals were found to form through internal nucleation, leading to bulk crystallization. These glasses had high bioactivity *in vitro*. Even when partially crystalline, they formed typical reaction layers, indicating bioactivity. In fact, sodium calcium silicate crystals were shown to transform *in vitro* into hydroxyapatite during soaking. However, crystallization should be avoided because it was shown to retard dissolution, bioactivity reactions and complicate fiber drawing process. Glass compositions having low alkali oxide content showed formation of wollastonite crystals on the surface, at about 300°C above the glass transition temperature. The wide range between glass transition and crystallization allowed viscous flow sintering of these compositions. These glasses also withstood the thermal treatments required for fiber drawing processing. Precipitation of calcium and phosphate on fibers of these glasses in SBF suggested that they were osteoconductive.

Glasses showing bioactivity crystallize easily, making their hot working challenging. Undesired crystallization can be avoided by choosing suitable compositions and heat treatment parameters, allowing desired product forms to be attained. Small changes in the oxide composition of the glass can have large effects and therefore a thorough understanding of glass crystallization behavior is a necessity for a successful outcome, when designing and manufacturing implants containing bioactive glasses.

SVENSK SAMMANFATTNING

Bioaktivt glas är ett intressant alternativ för implantatmaterial, på grund av att glassammansättningen är sådan att glaset lätt kan bilda kemiska bindningar till ben och styra bentillväxten. Vissa glassammansättningar har även bildat bindningar till mjukvävnad eller har antibakteriella egenskaper. Hittills är största delen av de kliniska tillämpningarna baserade på block, skivor, glaskross eller pulver. Dessutom har speciella produkter såsom porösa kroppar sintrade av glasskross eller fibrer tillverkade genom dragning från så kallade preformar eller smälta väckt intresse. De här formningsprocesserna är starkt viskositetsberoende, men kan störas av kristallisationen som förekommer vid samma temperaturområde.

I detta arbete undersöktes kristallisationstendensen och -kinetiken för en serie glas. Glassammansättningarna var valda att befinna sig inom gränserna för bioaktiva glas. De faktorer som påverkar kristallisationen och hur dessa står i samband med glasens sammansättningar undersöktes med termoanalys och upphettningsmikroskop. Sammansättningarna av de kristaller som bildades under isotermisk eller icke-isotermisk behandling analyserades med FEG-SEM/EDXA och röntgendiffraktion. Temperaturen, då sintring och fiberdragning kan ske utan störande kristallisation, bestämdes och de glassammansättningarna som är lämpliga för de här två ändamålen föreslogs. Bioaktiviteten av glasfibrer och delvis kristalliserade glasskivor undersöktes efter exponering i så kallad simulerad kroppsvätska. Tjockleken av de kisel-, kalcium- och fosfatrika skikt som bildats på glasytan vid exponering av simulerad kroppsvätska ansågs indikera bioaktivitet.

Resultaten visade att kristallisationsförmågan är starkt beroende av sammansättningen hos de undersökta glasen. Den viktigaste faktorn som påverkar kristallisationen verkade vara alkalioxidhalten: ju högre alkalioxidhalt, desto lägre kristallisationsförmåga. Den primära kristallfasen som bildades vid relativt låga temperaturer i dessa glas var natrium–kalcium–silikat. De här kristallerna visade sig bildas genom inre nukleidbildning, vilket kunde resultera i bulkkristallisation. Dessa glas bevarade hög bioaktivitet *in vitro*. Även i delvis kristalliserade former uppstod reaktionsskikt som indikerade bioaktivitet. Natrium–kalcium–silikatkristaller visades till och med att förvandla sig till hydroxiapatit i simulerad kroppsvätska. Kristallisationen borde ändå undvikas eftersom den tycks fördröja upplösning och reaktioner som har att göra med bioaktiviteten. Wollastonitkristaller bildades på ytan av glas med låg alkalioxidhalt vid en temperatur som var 300°C högre än glastransformationstemperaturen. Den långa räckvidden mellan glastransformationen och kristallisationen i dessa glas möjliggjorde viskös flödessintring (eng. viscous flow sintering). Dessa glas uthärdade också bättre termisk processering vid fiberdragningen. På basen av utfällning av kalcium och fosfat på fibrer i simulerad kroppsvätska antogs att fibrerna var bioaktiva.

Glas som visar bioaktivitet kristalliserar lätt, vilket gör deras värmebehandling utmanande. Oönskad kristallisation kan undvikas genom att välja lämpliga glassammansättningar och värmebehandlingsparametrar, vilka tillåter utformning av glas till önskade produktformer. Eftersom redan små ändringar i glasets oxidsammansättning kan vara avgörande, är en grundlig förståelse av glasets kristallisationsbeteende nödvändig för ett framgångsrikt resultat, när man konstruerar och tillverkar implantat av bioaktivt glas.

TABLE OF CONTENTS

1. INTRODUCTION

Glass is one of the oldest industrially manufactured materials. The properties of glass are achieved by carefully controlling the chemical composition and timing of heating and cooling, i.e. the process conditions, during manufacturing. In general, the development of commercial glasses aims at obtaining good chemical, thermal, optical, electrical or mechanical properties. The largest group of commercial glasses belongs to the soda-lime-silica system, i.e. the glasses used for containers, windows, tableware, and insulation. This system is readily worked at moderate temperatures, is chemically stable and can be manufactured from inexpensive raw materials [Kingery 1960]. Although this system is well-known it is still far from being simple. Alteration of the ratio of Na_2O, CaO and SiO_2 causes the glass to behave differently, for example with respect to temperature of melting. A general simplified composition in weight percent for conventional glasses in the soda-lime-silica system is 15 Na_2O, 13 CaO and 72 SiO_2. The same basic components: sodium oxide, lime and silica, are also present in bioactive glasses. Therefore, the comprehensive knowledge concerning conventional glasses can be applied to some extent to bioactive glasses.

The concept of bioactive glasses was invented by Professor Larry Hench and his co-workers in the early 1970s. The main idea was that an implant made of bioactive glass would be quickly and firmly fixed with tissue, before fibrous encapsulation takes place, and consequently would not necessarily require mechanical means of fixation nor a porous surface. This kind of fixation is possible due to kinetic modification of the glass surface that occurs upon implantation. The surface forms a biologically active hydroxycarbonate apatite (HCA) layer which provides a bonding interface for tissues. The HCA phase that forms on implants is chemically and structurally equivalent to the mineral phase in bone. It is that equivalence which is responsible for interfacial bonding, which is superior to that obtained with, for example, metal implants [Hench 1991]. The interface between the bioactive glass and bone is often so strong that removal of an implant necessitates breaking the surrounding bone or in some cases, the implant, but not the interface [Rawlings 1993].

The first bioactive glass described, Bioglass®, consists of 24.5 Na_2O, 24.5 CaO, 6 P_2O_5 and 45 SiO_2 given as weight percentages [Hench 1973]. Even today most of the bioactive glasses studied and clinically used have compositions near that of the original [Hench 2006]. The early bioactive glasses had three key compositional features that distinguished them from conventional soda-lime-silica glasses: (1) less than 60 mol % SiO_2, (2) high Na_2O and CaO contents, and (3) high CaO/P_2O_5 ratios. Most of the glasses satisfying these compositional parameters have been shown to bond to bone, some even to soft tissue, with the exception of compositions having substantially lower molar ratios of CaO to P_2O_5 [Hench 1991]. The first successful use of 45S5 Bioglass®, which has been in clinical use since 1985, was a replacement for the ossicles in the middle ear [Hench 1993, 2006]. Inspite of this success, bioactive glass products are limited to simple forms because of the strong tendency of this type of glasses to crystallize during heat-treatments, which are often required for manufacturing special products or shapes. Therefore, accidental crystallization (devitrification) is a likely problem during manufacture and should be avoided. Crystallization has also been reported to retard the development of the HCA phase and inhibit protein adsorption, both of which are thought to contribute to a decrease in bone bonding [Filho et al. 1996, El-Ghannam et al. 2001]. Over the years, the

bioactive response, as well as the working properties of bioactive glasses, have been adjusted by the addition of components such as B_2O_3, K_2O, and MgO [Andersson et al. 1988, Brink 1997]. The combined effect of different oxides in multicomponent systems is difficult to predict. However, some glasses in the system Na_2O-K_2O-MgO-CaO-B_2O_3-P_2O_5-SiO_2 have found clinical use and certain compositions are reported to have a wider working range than conventional bioactive glasses, thus allowing the drawing or spinning the of glass into fibers, or flame spraying into microspheres [Brink 1997, Ylänen et al. 1999]. These product forms provide many options for further processing into implants of different shapes.

Microspheres can be sintered into, for example porous implants. Optimum porosity of the implant can be controlled by using a narrow size fraction of spheres. Porous structures are advantageous because of the high reactive surface area and also because body fluids can flow through them, providing good biological conditions that lead to enhanced bone ingrowth [Ylänen et al. 1999]. Porous implants can also be produced by processing fibers in different ways. In addition, complex structures with interesting property combinations are possible, especially when combined with biocompatible polymers, which make them promising implant material candidates.

This study was a part of a project, in which textile processing methods were used to manufacture implant structures from bioactive glass fibers combined with biodegradable polymers. The ultimate goal was to develop bioabsorbable, load-bearing and easily formable scaffolds to be used in the field of bone tissue engineering instead of traditional metallic implants.

The aims of this thesis are:

- To determine the factors affecting crystallization of glasses with compositions within the range of bioactivity and its possible effect on *in vitro* behaviour.

- To establish which glass compositions are suitable for sintering or fiber drawing purposes and at which temperatures these processes can take place without crystallization interfering.

This thesis is based on the following publications. They will be later referred to in the text by their Roman numerals:

I. The sintering range of porous bioactive glasses, H. Arstila, L. Fröberg, L. Hupa, E. Vedel, H. Ylänen and M. Hupa, Glass Technology, 2005, **46** (2), p. 138-141.

II. Predicting physical and chemical properties of bioactive glasses from chemical composition. Part II: Devitrification characteristics, H. Arstila, E. Vedel, L. Hupa and M. Hupa, *accepted* to Glass Technology: European Journal of Glass Science and Technology: Part A.

III. Factors affecting crystallization of bioactive glasses, H. Arstila, E. Vedel, L. Hupa and M. Hupa, Journal of the European Ceramic Society, 2007, **27** (2-3), p. 1543-1546.

IV. Influence of heat treatment on crystallization of bioactive glasses, H. Arstila, L. Hupa, K. H. Karlsson and M. Hupa, Journal of Non-Crystalline Solids, 2008, **354**, p. 722-728

V. Liquidus temperatures of bioactive glasses, H. Arstila, M. Tukiainen, S. Taipale, M. Kellomäki and L. Hupa, Advanced Materials Research, 2008, **39-40,** p.287-292.

VI. *In vitro* bioactivity of partially crystallized glasses, H. Arstila, L. Hupa, K.H. Karlsson, M.Hupa, Glass Technology: European Journal of Glass Science and Technology Part A, August 2007, **48** (4), p. 196-199.

VII. *In vitro* reactivity of bioactive glass fibers, H. Arstila, M. Tukiainen, L.Hupa, H. Ylänen, M. Kellomäki and M. Hupa, Advances in Science and Technology, 2006, **49,** p. 246-251.

Results related to the thesis are also presented in

Measuring the devitrification of bioactive glasses, H. Arstila, E. Vedel, L. Hupa, H. Ylänen, M. Hupa, Key Engineering Materials, 2004, **254-256**, p. 67-70.

Bioactive glass compositions suitable for repeated heat treatments, H. Arstila, D. Zhang, E. Vedel, L. Hupa, H. Ylänen and M. Hupa, Key Engineering Materials, 2005, **284-286**, p. 925-928.

High temperature properties of bioactive glasses, L. Hupa, K. H. Karlsson, E.Vedel, H. Arstila, B. Jonson, Proceedings of the XX A.T.I.V. Conference, Parma Italy, 2005.

Control of the forming properties of bioactive glasses, E. Vedel, H. Arstila, D. Zhang, L. Hupa and M. Hupa, Glass Technology: European Journal of Glass Science and Technology Part A, August 2007, **48** (4), p. 191-195.

Potential use of craniosynostotic osteoprogenitors and bioactive scaffolds for bone engineering, L. Santos-Ruiz, D. J. Mowatt, A. Marguerie, M. Tukiainen, M. Kellomäki, P. Törmälä, E. Suokas, H. Arstila, N. Ashammakhi and P. Ferretti, Journal of Tissue Engineering and Regenerative Medicine, 2007, **1**(3), p. 199-210.

In vitro Behavior of Fiber Bundles and Particles of Bioactive Glasses, D. Zhang, H. Arstila, E. Vedel, H. Ylänen, L. Hupa and M. Hupa, Key Engineering Materials 2008, **361-363** p. 225-228.

Predicting Physical and Chemical Properties of Bioactive Glasses from Chemical Composition. Part I: Viscosity Characteristics, E. Vedel, H. Arstila, H. Ylänen, L. Hupa and M. Hupa, *accepted* to Glass Technology: European Journal of Glass Science and Technology: Part A.

Predicting Physical and Chemical Properties of Bioactive Glasses from Chemical Composition. Part IV: Tailoring compositions with desired properties, E. Vedel, D. Zhang, H. Arstila, L. Hupa and M. Hupa, *accepted* to Glass Technology: European Journal of Glass Science and Technology: Part A.

Contribution of the author

The author's contributions to the papers on which this thesis is based are the following:

I. The author was responsible for the DTA, HSM and XRD analyses of the glasses and the responsible author of the publication.

II. The author was responsible for the DTA, HSM, SEM-EDX and XRD analyses of the glasses, for evaluating the test results and for modelling of properties as functions of the glass composition. The heat-treatments prior to analysis were also performed by the author. The author was the main writer of the publication.

III. The author was responsible for the experimental design of the study and evaluation of the test results. The author was the main writer of the publication.

IV. The author was responsible for evaluating the results and the main writer of the publication.

V. The author was responsible for the DTA, HSM, SEM-EDX and XRD analyses of the glasses, drawing fibers and for evaluating the test results. The author was the main writer of the publication.

VI. The author was responsible for evaluating the results and the main writer of the publication.

VII. The author was responsible for the all the practical laboratory work as well as the analyses of the results. The author was the main writer of the publication.

2. LITERATURE REVIEW

2.1. Structural theories of glass formation

Glass is a substance that can be defined in many different ways. Two general definitions are that glass is an amorphous, i.e. structureless solid or that glass is a non-crystalline solid [Pye 1972]. Every glass exhibits also a region of glass transformation behavior [Shelby 1997]. A number of materials fulfill these two requirements and can be called glass, but what is considered traditional glass is usually a combination of silica and other oxides. The structure of oxide glasses is often described by the well-known theory of Zachariasen (1932), which was later confirmed by Warren (1941). At least for conventional glasses, a large number of properties can be explained or predicted by the Zachariasen-Warren concept. Also, the surface reactive nature of bioactive glasses and their crystallization tendency can be understood to some degree by the theory.

According to the Zachariasen-Warren theory, a disordered network is built from SiO_4 tetrahedron units joined by oxygen atoms in every corner, but the mutual orientation of the consecutive tetrahedra is variable (Fig 1). Zachariasen established rules to classify different oxides or ions according to their coordination properties. Cations, which form the vitreous network of the glass together with oxygen, are called network formers. Other oxides that do not participate directly in the network, but rather fill the cavities, are called network modifiers. The latter are essentially the oxides of the alkali metals and alkaline earths. A third group are intermediate oxides that can function either as glass-formers or as modifiers depending upon the glass composition [Zarzycki 1991].

Stanworth (1952) improved Zachariasen's model by taking into account the correlation between electronegativity of oxides relative to oxygen and their ability to form glass. He used this approach to categorize glasses, so that group 1 corresponds to glass formers and group 3 to glass modifiers. The oxides relevant to this work are classified according to Zachariasen's rules and electronegativity relative to oxygen in Table 1. The table shows that the electronegativity of glass formers is around 2, while glass modifiers have an electronegativity around 1.

Table 1. Classification of the oxides relevant to this work according to glass forming ability and electronegativity relative to oxygen based on Zachariasen's and Stanworth's theories.

Glass formers / Group 1						*Glass modifiers / Group 3*							
P	2.1	B	2.0	Si	1.8	Mg	1.2	Ca	1.0	Na	0.9	K	0.8

A typical glass modifier is Na_2O. The Na^+ cations occupy the cavities between the tetrahedral, leaving oxygen ions to increase the O:Si ratio, which leads to progressive breakage of the SiO_2 network. A direct effect of breaking down the network is lowered viscosity [Kingery 1960]. The Si-O-Si bridge rupture mechanism leads to a loosened network structure with two types of oxygens: an oxygen bonded to two Si is called a bridging oxygen (BO) and an oxygen bonded to one Si is called a non-bridging oxygen (NBO). A schematic presentation of the functions of different ions in glass structure is given in Figure 2.

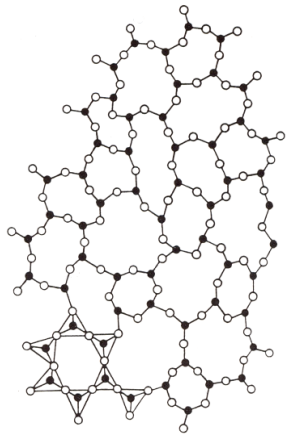

Figure 1. Two dimensional drawing of disordered network structure of SiO_4 building blocks in SiO_2 glass, after Zachariasen and Warren [Vogel 1994].

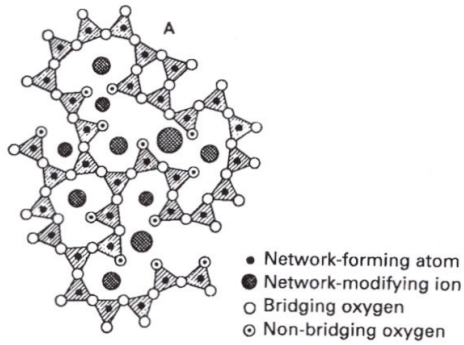

Figure 2. Two dimensional drawing of arrangement and functions of the different ions in glass [Davison 2003].

The same mechanism applies to the introduction of an oxide of a divalent cation, for example CaO. In this case, a single cation Ca^{2+} is sufficient to compensate for the two negative charges of the non-bridging oxygens. Bridges in the fundamental network start to break near these large cations causing increased mobility of SiO_4 and thereby a decrease in both viscosity and melting rate [Vogel 1994].

Dietzel proposed an extension of the network theory in 1942. He introduced the term "field strength" to characterize the effect of a single cation, assuming that the anion is oxygen. For example, on cooling of a binary silicate melt, two cations compete with respect to their oxygen environment in order to achieve densest packing. If the field strength of both cations is approximately equal, demixing will usually occur, leading to two pure oxide phases. If, however, field strengths differ, the oxygen ions will be used predominantly for densest packing around the cation with the higher field strength. The cation with a lesser field strength must be satisfied with a higher coordination number in comparison to the anion complex formed by the other cation. In general, in a system containing two network formers, crystallization of the melt is more likely the greater the difference in the field strengths [Rawson 1980]. This explains why combinations of SiO_2, B_2O_3 and P_2O_5 in one melt show a decreased tendency toward glass formation, leading to immiscibility and phase-separated glass [Vogel 1994].

2.2. Kinetic theories of glass formation and crystallization

Structural theories may describe glass formation in detail, but kinetic theories are applicable to most known glass systems, unlike structural theories. Both glass formation and crystallization are kinetic phenomena and are therefore discussed here in the light of kinetic theories. The manufacture of glass is based on cooling the melt so that it will not attain the crystalline low-energy state it strives to assume. The temperature at which supercooled liquid turns into glass is called the transition

temperature or the glass transformation temperature T_g. The liquidus temperature (T_L) is the temperature below which a single liquid phase is no longer thermodynamically stable [Rawson 1980]. Most glass-forming melts show some sign of crystallization if held just below the liquidus temperature long enough for structural arrangements to occur. Crystallisation can occur either on cooling or reheating, but it always involves two individual kinetic processes: formation of submicroscopic nuclei, and their growth into macroscopic crystals. These two processes are called nucleation and crystal growth, respectively.

Nucleation

The classical nucleation theory (CNT) was originally developed to describe liquid droplet nucleation from vapour as described by Weinberg (1992): *The theory, in its original form, consists of two parts: 1) a thermodynamic expression for the free energy of formation of a liquid droplet, and 2) a kinetic part which governs the size evolution of a droplet. The first part leads to concept of critical radius and the definition of the nucleus, while the second leads to an expression for the nucleation rate*. The nucleation of a glass melt commences from small, thermodynamically unstable regions, which are called "embryos". They form momentarily as a result of random fluctuations, but disappear as quickly as they are formed. The fluctuations may differ in size, form, structure or composition, but in the simplest model it is assumed that the embryos have a uniform structure and properties that are similar to those of the future phase, and differ only in size and form (which can be assumed to be spherical). An embryo will become a stable nucleus if fluctuations emerge which produce a crystalline region exceeding the critical size [Rawson 1980]. Once a nucleus of sufficient size is formed, it tends to grow further by the addition of one or several units through a diffusion mechanism until the supersaturation is relieved [Vehkamäki 2006]. This leads to a decrease in free energy [Zarzycki 1991]. The rate at which nuclei form, i.e. the nucleation rate, depends on both a thermodynamic and a kinetic factor [Rawson 1980]. Classical nucleation theory is based on many assumptions and is often used to describe homogenous nucleation in simple single-component systems, although it can be applied to multicomponent systems as well [Vehkamäki 2006]. However, the applicability of the CNT to prediction of nucleation rates in glasses has been a matter of widespread controversy. In practice, measuring nucleation rates is both difficult and time consuming, which is why the commonly accepted CNT assumption that the maximum nucleation rate is just at or a little above T_g is, in spite of all, used [Fokin et al. 2003].

Nucleation which occurs in a totally random manner throughout the entire system is said to be homogenous. The necessary condition for this is that all volume elements of the initial phase must be structurally, chemically and energetically identical. In heterogenous nucleation, the nucleus develops on the surface of a foreign solid such as container walls, impurity particles or structural imperfections. The function of such nucleating substrates is to reduce the barrier to nucleation represented by the surface energy. Heterogeneous nucleation is so difficult to avoid that totally homogeneous nucleation is rarely attainable [Zarzycki 1991].

An often-used theory to describe the kinetics of homogenous and heterogenous nucleation is called the JMAK theory after its developers Johnson, Mehl, Avrami and Kolmogorov. The theory is based on an equation which is universally applicable to glass-ceramics [Höland and Beall 2002]. However, Weinberg and colleagues have

questioned the theory's validity for non-spherical particles, e.g. needle-like crystalline phases and proposed models describing the kinetics of crystallization of highly anisotropic particles [Birnie and Weinberg 2000]. They have also critically evaluated the assumptions related to classical nucleation theory (Weinberg et al. 2002).

Volume crystallization can result from either homogeneous or heterogeneous nucleation [Paul 1982]. For example, gas bubbles that are spread evenly throughout the whole volume provide heterogeneous nucleation sites, enhancing the risk of volume crystallization. However, experience with glass-forming liquids has indicated that crystal nucleation almost always takes place at external surfaces [Kingery 1960]. For example, when a piece of glass is heat-treated (between T_g and T_L), such that the surface is exposed to air, a favorable interface for nucleation is created. Crystals, which are often needle-like in shape, start to grow inwards from the surface as a result of the initial heterogeneous nucleation [Rawson 1980]. The molecules on the surface feel less attraction from their neighbors than the molecules in the interior, since they are not fully surrounded by other molecules [Vehkamäki 2006]. Therefore there is a strong possibility of nucleation on the surface continuing to crystal growth along the interface. This whole process is called surface crystallization [Paul 1982].

Crystal growth

The actual crystal growth process begins when a nucleus proceeds to grow by the successive addition of atoms from the surrounding phase. This leads to the formation of a crystalline particle which grows at a certain rate, known as the crystal growth rate, at the expense of the surrounding phase [Zarzycki 1991]. Ions bind together to form molecules, which form chains and finally a lattice [Vogel 1994]. A number of models have been proposed to describe the crystal growth process. Each is based on a different view of the interface and the sites available for growth. In the normal growth model, the interface must be rough on an atomic scale and be characterized by a large fraction of step sites where atoms can preferentially be added and removed. When the interface is relatively smooth but still imperfect on an atomic scale, the growth takes place in steps which proceed spirally. This process is called screw dislocation growth. It is suggested that this is a good model to describe crystal growth in silicate glasses [Fokin et al. 2005]. If the interface is, however, perfect (free of intersecting screw dislocations) growth takes place at sites provided by two-dimensional nuclei formed on the interface and will proceed by distribution of a monolayer across the surface until the surface is covered [Kingery 1960, Paul 1982]. This process is called surface nucleation growth, but is not generally observed for silicate systems [Paul 1982].

A simple schematic figure is often used to describe how nucleation and crystal growth rates depend on temperature (Fig 3). If the glass melt is cooled rapidly enough (supercooling) to below equilibrium solubility (the liquidus temperature), it enters a metastable zone in which nuclei do not form. Crystals can, however grow if nucleated before supercooling [Uhlmann and Kreidl 1982]. The more likely region for crystallization to occur, both during cooling and reheating, is under the overlapping curves for nucleation and crystal growth (Fig. 3). If there is a substantial overlap of the curves and both nucleation and crystal growth rates are high, total crystallization cannot be avoided [Zarzycki 1991].

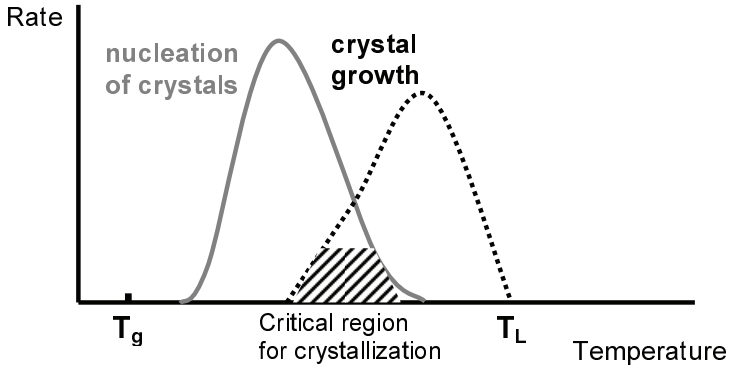

Figure 3. Effect of temperature on rates of nucleation and crystal growth on heating glass, redrawn from Uhlmann and Kreidl 1982.

Reheating provides energy for the structural elements in glass to rearrange again. The nuclei, which have formed either by homogeneous or heterogeneous nucleation during cooling, can grow further while at the same time new nuclei can form. Since the size of the critical nucleus increases with increasing temperature, some nuclei can become oversized and melt out [Uhlmann and Kreidl 1982]. Still, the presence of suitable nuclei for crystal growth is more probable upon reheating, making the overall risk for crystallization higher.

Studying crystallization kinetics

Differential thermal analysis (DTA) is often used to determine the characteristic temperatures associated with particular transitions that occur during heating of glasses. During analysis the temperature is varied linearly as a function of time and the difference between the glass specimen and an inert reference is measured. The first measurable effect is the glass transition temperature $\mathbf{T_g}$, which occurs at a fairly low temperature. The temperature $\mathbf{T_g}$ corresponds to the endothermic inflection point on the heating curve, as shown in Figure 4, that is caused by the increase in heat capacity. The values for same glass composition even can vary, because there is no unified method for determining Tg. At a slightly higher temperature an exothermic peak is usually observed, which is due to crystallization. More crystallization peaks are possible if several separate crystallizing phases are present [Wilburn and Dawson 1972]. The melting of crystals causes an endothermic peak, or more precicely “a valley of peaks”, occurs at relatively high temperatures. The liquidus temperature corresponds to the offset of the endothermic peak [Ray 1979].

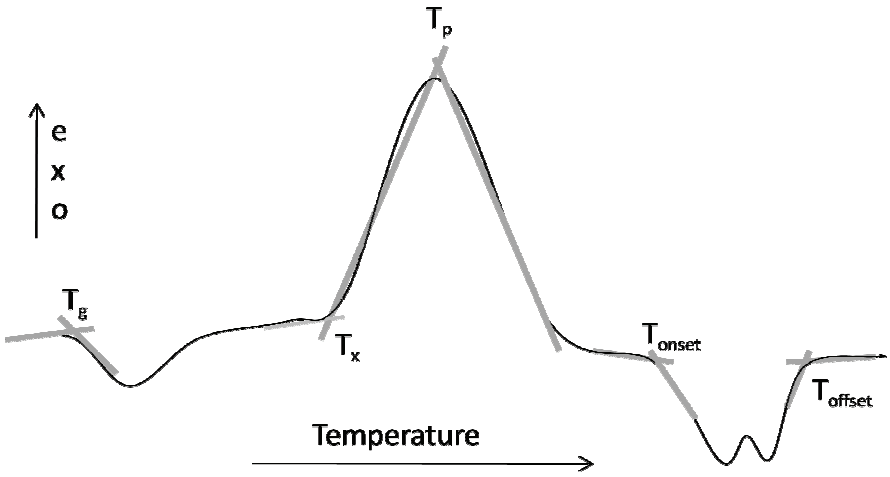

Figure 4. A schematic representation of an ideal DTA heating curve of a glass sample.

The area of the exothermic peak is related to the rate of crystallization. Although powdered samples are known to crystallize readily due to their high surface area, the effect on the crystallization rate is primarily to make the peak wider, thereby shifting the onset of crystallization to lower temperatures. Relative rates of crystallization of different glasses can be compared provided that the different glasses are powdered to the same particle size [Wilburn and Dawson 1972]. If bulk samples are used and only surface crystallization occurs, no exothermic peak is expected at all on the DTA curves owing to the low surface area of the sample [Branda et al. 1984]. A DTA study of Bioglass® with differerent particle sizes showed that bulk samples caused only one exothermic peak while powdered samples gave rise to two peaks, which were attributed to different crystallization mechanisms, namely surface and bulk crystallization [Chatzistavrou et al. 2006].

In order for crystallization to commence, a certain activation energy is required. The tendency to crystallize can be determined by comparing the activation energies of different glass compositions. The ease of forming different crystal types can, however, vary. Activation energy can be determined by DTA using the so-called Kissinger method or a modification thereof, when a majority of the nucleation occurs during the DTA measurement [Augis and Bennett 1978]. In this method, the peak temperatures ($\mathbf{T_p}$) obtained with different heating rates ($\boldsymbol{\alpha}$) are used to calculate values for $\mathbf{\ln (\alpha / T_p^2)}$ which are plotted against $\mathbf{1 / T_p}$ values. The slope of this line gives the relationship between activation energy for crystal growth (**E**) and the gas constant (**R**). However, in order to attain meaningful activation energies the crystallization mechanism should be known [Matusita and Sakka 1980]. When the activation energy is determined, the Avrami parameter **n**, which indicates shape and dimensionality of the crystal growth, can also be calculated, according to equation $\mathbf{n = 2.5\ RT_p^2 / \Delta\tau\ \Delta E}$, where $\boldsymbol{\Delta\tau}$ is the full width of the DTA exothermic peak at its half maximum. One-dimensional crystal growth should give **n** = 1, two dimensional **n** = 2 and three-dimensional bulk crystallization **n** = 3. Values of 1-2 correspond to surface

crystallization [Marotta et al. 1978, 1982]. An example of determining **ΔE**, **Δτ** and finally the Avrami parameter **n** is given in the Results section of this work.

Other statistical measures of crystallization, which are often used to describe crystallization that takes place on cooling a liquid, can also be used to describe glass crystallization on reheating. The assumption is that the thermal stability of a glass on subsequent reheating is directly proportional to the ease of its formation [Uhlmann and Kreidl 1983]. To quantify glass formability the cooling rate required to make a glass from the melt is often calculated. The cooling rate that produces the lowest detectable degree of crystallization is called the critical cooling rate for glass formation. It can be estimated from the time-temperature-transformation (TTT) curves which define the relationship between the temperature and the time interval required to reach a given degree of crystallization. Each TTT curve has an inflection point or nose. It represents the least time required to form a given degree of crystallinity. Both nucleation and crystal growth are much faster at this point than at other temperatures [Uhlmann and Kreidl 1982]. From this inflection a rough estimate of the critical cooling rate can be determined [Vogel 1994]. However, TTT curves require detailed kinetic information and abundant experimental data and still an accurate critical cooling rate may be difficult to determine [Uhlmann and Kreidl 1982]. Some simple correlations have been proposed to evaluate the probability of glass crystallization.

The stability of glasses against crystallization upon reheating is often described with relative values calculated from the temperatures of glass transition, liquidus and crystallization [Hruby 1972, Zanotto 1987]. The equation $\mathbf{T_g / T_f = 2/3}$ (T_f corresponding to fusion temperature) holds quite well for many systems ranging from organic polymers even to silicates [Sakka and MacKenzie 1971]. This empirical rule can even be extended to stand for liquidus temperatures $\mathbf{T_L}$ instead of $\mathbf{T_f}$ and is often referred to as the reduced glass transition temperature $\mathbf{T_{RG}}$ (or **Tgr**). According to Turnbull [1965] a good glass former is one for which the critical $\mathbf{T_{RG}}$ is equal to or larger than 2/3. Otherwise, crystal nucleation dominates during cooling, which prevents the glass formation. The glass stability is also expected to increase with increasing $\mathbf{T_g / T_L}$ [Branda et al. 1984]. When crystallization occurs, the same correlation has been used to estimate whether it is internal or surface crystallization. With $\mathbf{T_{RG}}$ values less than 0.58, internal nucleation is seen [James 1985, Wakasugi et al. 1999]. $\mathbf{T_{RG}}$ is a good tool for understanding the general trends of nucleation and time-lag temperature dependencies [Fokin et al. 2003].

Another way to approximate glass stability is to measure the difference between crystallization temperature and glass transition as expressed by the equation temperature $\mathbf{\Delta T = T_{p/x} - T_g}$. $\mathbf{T_x}$ refers to the onset of crystallization, while $\mathbf{T_p}$ is the peak temperature of maximum crystallization. Glass transition and especially crystallization temperatures are dependent on the cooling rate originally used to form the glass, as well as on the heating rate and measurement technique. However, this quantity serves as an indicator for further glass stability analysis [Drexhage et al. 1983].

A significant correlation between the so-called Hruby parameter $\mathbf{K_{gl}}$ and glass-forming tendency, estimated by critical cooling rates, has been suggested by Cabral et al. (1997). This parameter is based on the equation $\mathbf{K_{gl} = (T_c - T_g) / (T_L - T_p)}$. The Hruby parameter can be used to estimate the glass-forming ability for glasses that

exhibit volume nucleation: the higher the $\mathbf{K_{gl}}$ values, the better the glass formability [Cabral et al. 1997]. In general, glass stability parameters that consist of three characteristic temperatures show excellent correlation with glass forming ability parameters, but if only two temperature values are used the correlation is rather poor [Nascimento et al. 2005].

The effect of different oxides on glass properties

Glasses can be made over a wide range of compositions in the alkali-silicate systems. The range of glass-forming compositions is continuous from silica itself up to about 50 mol-% of the alkali oxide. With addition of alkali oxides, the eutectic composition is approached, which usually reduces the liquidus temperature, thereby increasing stability of the glass [Rawson 1980]. However, even in the perfectly clear ternary (Na_2O-CaO-SiO_2) glasses, the alkali ions may not be uniformly distributed throughout the structure. Although a glass may seem to be apparently homogenous, the alkali ions may tend to form clusters [Rawson 1980, Vogel 1994]. A separation into an alkali-rich and a SiO_2-rich phase will facilitate leaching of the alkali-rich phase by water or air [Vogel 1994]. On the one hand, this kind of solubility is a requisite for bioactive reactions, but on the other hand it may reduce their long-term reliability [Andersson and Karlsson 1990A]. Andersson et al. (1988) investigated the role of additional oxides such as B_2O_3 and Al_2O_3 hoping to be able to produce bioactive glasses with reduced solubility. However, the alumina was found to retard or inhibit the transformation of osteoid into bone and therefore the amount of alumina in glass compositions intended for implant purposes should not exceed 1.6 wt-%.

In the original bioactive glasses, six wt-% P_2O_5 was added to the basic soda-lime-silica glass formulas in order to make them equivalent to hydroxyapatite with respect to calcium and phosphate [Hench 2006]. However, studies with phosphate free glasses showed that, for apatite formation in biological environments, more important than the P_2O_5 content is the availability of non-bridging oxygens and a flexible silica structure [Andersson et al. 1990c, Kim et al. 1995]. The importance of non-bridging oxygen ions during surface chemical processes has been confirmed by the calculations of Koga et al. (2003). Structural analysis with MAS-NMR showed that in bioactive glasses phosphate is in the orthophosphate (PO_4^{3-}) form and associated with removing sodium and calcium ions from a network modifying role, resulting in a reduction in the number of non-bridging oxygens [Lockyer et al. 1995, Elgayar et al. 2005]. Orthophosphates were assumed to be present due to amorphous phase separation, but no evidence of such was found.

The calcium to phosphate ratio also has a significant influence on nucleation and crystallization behavior during heat treatments. In a study of apatite glass ceramics in the multicomponent system SiO_2-Al_2O_3-P_2O_5-CaO-CaF_2, it was found that if the calcium to phosphate ratio is 1.67, corresponding to that of apatite, bulk nucleation was favored [Clifford et al. 2001]. Non-ideal ratios exhibited surface nucleation of fluorapatite. Due to the presence of P_2O_5, glass 45S5 deviates from the ideal stoichiometric composition and can therefore never be totally crystallized. Even in optimal crystallization conditions, the maximum crystallinity degree is 77.4 wt-% for 45S5 [Chen et al. 2006a]. Therefore some residual glass and non-bridging oxygens are always present in glass derived ceramics.

A common glass additive is K_2O, which has a special ability to harden the glass [Uhlmann and Kreidl 1983]. However, in a mixed Na/K glass, for example, Na^+ ions move more easily into sites previously occupied by Na^+ ions than those previously occupied by K^+ ions, and vice versa [Ingram et al. 1992]. The gradual replacement of the two ions, leading to ionic aggregation and immiscibility processes in a melt as the temperature decreases makes many glass properties show an abnormal change, which is called the mixed alkali effect. For this to occur, the total alkali content should be at least 10 mol-%. It has been experimentally observed that the mixed alkali effect appears to be especially strong when the two alkali ions present in the glass have very similar field strengths, as in the combination of sodium and potassium, but it also appears when an alkali ion and alkaline earth ion or two alkaline earth ions are combined in a glass [Vogel 1994]. To improve durability, the alkali content of conventional glasses is usually kept under 14% [Uhlmann and Kreidl 1983].

The value for the maximum rate of crystal growth may change markedly with even minor changes in glass composition. In general, alkali and alkaline earth oxides have a tendency to increase the crystal growth rate to some extent [Rawson 1980]. The problems with crystallization in sheet glass production have necessitated replacing some CaO with MgO. A typical average soda-lime glass can contain up to 4% MgO [Vogel 1994]. MgO reinforces the structure of complex silicate glasses, revealing the formal character of the network-modifying concept, which fits only larger or monovalent cations. MgO reduces the liquidus temperature slightly, reduces the maximum crystal growth rate and increases elasticity. Therefore it is best suited to special purposes such as glass compositions for fiber drawing purposes. However replacing CaO with MgO shortens the temperature range, when glass processing usually takes place [Uhlmann and Kreidl 1983].

Crystalline phases

Heat treatments provide favorable conditions for crystal formation. Even in the most persistent glasses, atoms can re-arrange at the nucleation stage in a defined and periodic manner that defines the crystal structure. Depending on the parent glass composition and thermal conditions, the crystalline structure takes form. However, even if most of the atoms take part in crystallization and no residual glass or liquid is assumed to exist, there might be several possible outcomes. As with carbon turning into graphite or diamond, SiO_2 can form, at least theoretically, quartz, tridymite or cristobalite, depending on the conditions. If the Na_2O-SiO_2 binary system is considered, crystalline forms of $Na_2O{\cdot}SiO_2$, α-$Na_2O{\cdot}2SiO_2$ and β-$Na_2O{\cdot}2SiO_2$ are possible. In the ternary system $Na_2O{\cdot}SiO_2$-$CaO{\cdot}SiO_2$-SiO_2 the options for crystallization products are multiplied as seen in Figure 5 [Morey 1954]. The primary crystalline phases within the glass forming region of this system are outlined with darker lines. Basically, compositions with over 75 weight-% SiO_2 can only give rise to crystalline silica. With less SiO_2 and roughly 0-20 weight-% Na_2O, α- and β-wollastonite ($CaO{\cdot}SiO_2$) or devitrite ($Na_2O{\cdot}3CaO{\cdot}6SiO_2$) are possible primary crystalline phases. The arrangement of atoms in $CaO{\cdot}SiO_2$ is fairly simple. If Na_2O content is higher than 20 weight-%, more complicated structures of sodium-calcium-silicates can form. The actual ratio of sodium oxide, lime or silica in these crystal phases and their identification with X-ray diffraction analysis is rather difficult, because several strong peaks are common to two or more of the compounds [Backman et al. 1990, 1997]. Continuous compositional change in the crystals during the course of crystallization for a glass which is just left of the stoichiometric

$Na_2O{\cdot}2CaO{\cdot}3SiO_2$ ratio has been reported recently by Fokin and Zanotto (2006). The solution found between the solid compounds $2Na_2O{\cdot}CaO{\cdot}3SiO_2$ and $Na_2O{\cdot}2CaO{\cdot}3SiO_2$ can be the cause of peculiar crystal formation and has been taken into consideration in thermodynamic modeling [Pelton and Wu 1999, Karlsson and Backman 2005].

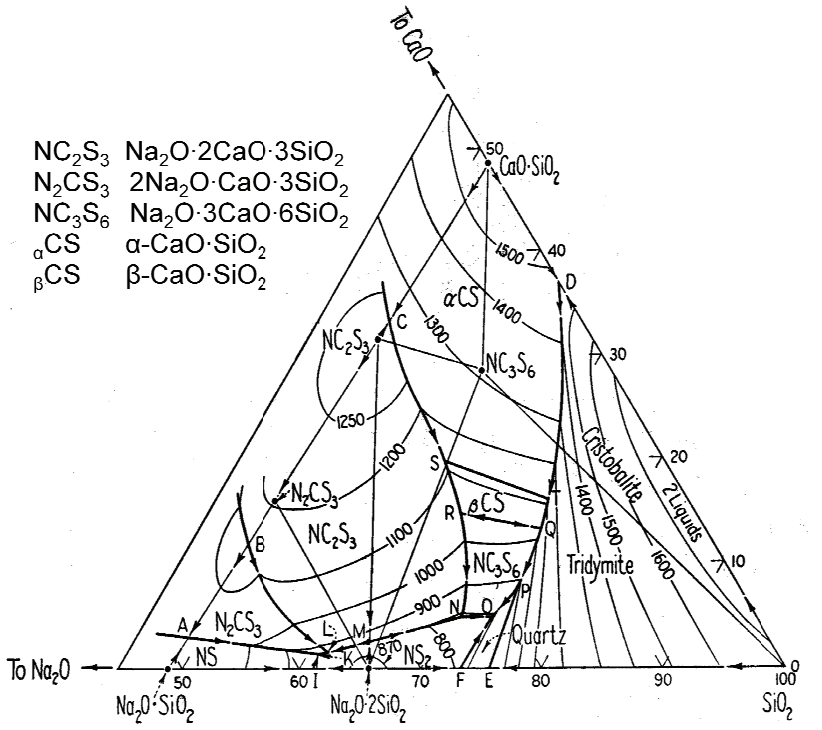

Figure 5. The high SiO_2 corner of the ternary Na_2O-CaO-SiO_2 system [from Phase Diagrams for Ceramists Levin et al. 1964].

Figure 5 also shows the curved liquidus lines within the primary crystalline fields. They describe the gradual melting of the different crystalline phases when relative proportions of the various compounds differ. The compositions of pure crystalline compounds and their crystalline habits, melting, decomposition or inversion temperatures are listed in Table 2. Where complex glasses are concerned, the simple phase diagram is of very limited use for determining the liquidus temperature, because the phase boundaries can move rapidly when other components are added [Backman et al. 1990]. Therefore, experimental models provide the best solution for predicting the relationship between liquidus temperature and composition [Backman et al. 1997].

In bioactive glasses different crystal types can form, depending on the composition. Bioactive glass 45S5 has been reported to crystallize to $Na_2Ca_2Si_3O_9$ ($2Na_2O{\cdot}CaO{\cdot}3SiO_2$) during heating with an activation energy of 350 kJ/mol [Peitl et al. 2001, Clupper and Hench 2003, Chen et al. 2006A]. An apatite-like phase was also observed to grow simultaneously with the sodium calcium silicate phase [Chatzistavrou et al. 2006]. In another crystallization study of glass formulations of

the Hench type (Na_2O-CaO-SiO_2-P_2O_5) the outcome of crystallization was $CaSiO_3$, $Na_2CaSi_3O_9$ and $Na_4Ca_3Si_6O_{16}(OH)_2$ crystal phases giving activation energy values between 196 and 782 kJ/mol [Rizkalla et al. 1996]. The melting of crystal phase $Na_2Ca_2Si_3O_9$ in glass 45S5 has been reported to occur in the range of 1100-1250°C [Chatzistavrou et al. 2006, Lefebvre et al. 2007]. Crystallization has been shown to retard the reactions indicating bioactivity [Filho et al. 1996, El-Ghannam et al. 2001].

Table 2. Compositions of different crystalline compounds in wt-% and their melting (m), inversion (i) or decomposition (d) temperatures and crystal habit [Morey 1954].

Compound	*CaO*	*Na_2O*	*SiO_2*	*Crystal habit*	*Temp [°C]*
$Na_2O{\cdot}2CaO{\cdot}3SiO_2$	31.6	17.5	50.9	equant	1284 (m)
$2Na_2O{\cdot}CaO{\cdot}3SiO_2$	15.6	34.4	50.0	octahedra	1141 (d)
$Na_2O{\cdot}3CaO{\cdot}6SiO_2$	28.5	10.5	61.0	prisms	1060 (d)
α-$CaO{\cdot}SiO_2$	48.3		51.7	hexagonal plates	1540 (m)
β-$CaO{\cdot}SiO_2$	48.3		51.7	needles	1150 (i)

2.3. Bioactivity of glasses

Bioactivity of glasses generally refers to their ability to form a chemical bond with bone. This happens as a result of a series of complex reactions on the glass surface in aqueous environments both *in vitro* and *in vivo* [Hench 1991]. The first reactions occur regardless of whether the environment is a real living body or a simulated aqueous one. According to Hench (1974, 1991), the alkali ions and PO_4^{3-} start to dissolve from the glass and are replaced by hydrogen or hydronium ions from the environment, resulting in an increase in pH of the solution. The silica network of bioactive glass starts to dissolve due to attack by the hydroxyl ions. Soluble silica is lost from the glass to the surrounding environment, and Si-OH or $Si(OH)_4$ groups are formed at the surface of the glass. In order to form a SiO_2 rich surface layer, condensation and repolymerisation must occur. After this, calcium phosphate precipitation commeces on top or within the SiO_2 rich layer. The SiO_2 layer continues to grow by diffusion-controlled alkali ion exchange. Soluble calcium phosphates, originating from the glass or the surrounding environment, promote the growth of a CaO-P_2O_5 –rich layer. Finally, the carbonate-containing hydroxy apatite crystallizes to resemble hydroxyapatite of bone. These first stages happen within hours or days, depending on the glass composition and the structure of the implant.

In vitro testing of bioactivity is often done by using a simulated body fluid (SBF) as an acellular environment. The most common method uses the simulated body fluid developed by Kokubo, which contains all the essential inorganic components of human body fluids [Kokubo et al. 1990, 1992]. As an indication of bioactivity the reactions described above should occur. The *in vitro* bioactivity is assumed to correlate with *in vivo* bioactivity, because many authors have verified the reaction layer formation *in vivo* [Hench 1991, Andersson et al. 1990b, Brink et al. 1997b, Ylänen et al. 2001]. However, the rate of the surface reactions has been reported to be slower *in vivo* due to the delaying effect of serum proteins [Kaufmann et al. 2000].

The simple relationship between bioactivity and composition was determined by altering the ratio of Na_2O, CaO and SiO_2 and keeping the P_2O_5 amount constant [Hench 1991]. Bone bonding and even soft tissue attachment was achieved with

glasses close to the 45S5 composition. This work gave valuable information on the compositions required for bioactivity. The amount of SiO_2 has been thought to be crucial, because the dissolution rate decreases if the SiO_2 content is > 60 mole%, due to the larger number of bridging oxygen bonds in the glass structure, which has been verified with apatite-wollastonite (A-W) glasses [Hench and Wilson 1993]. However, gel-derived glasses having up to 85 mole% SiO_2 have also been shown to be bioactive [Li et al. 1991]. Another important factor has been suggested to be the ratio of calcium to phosphorous, which should be between 1.05 and 1.67 for an ideal synthetic bioceramic [Tas 2003].

In multi-component systems it is difficult to find a simple relationship between composition and bioactivity. Phenomenological models can be of great help. Andersson et al. (1988) studied the bone bonding behavior of nine glasses by implantation of glass cylinders in rabbit tibia. Based on to the results a model was proposed. The formation of Si-rich and calcium phosphate layers on glass plates after soaking in SBF was measured by Zhang et al. (2005). A phenomenological model was calculated based on the results with 30 glass compositions, which are the same as those used in the present study [Zhang et al. 2008].

The rate of bone bonding can be enhanced by rational design of the implant form. A traditional way to attain bone ingrowth into the implant is to have pores in the implant structure. The presence of interconnected pores having pore sizes in the range of 150 to 700 μm facilitates complete invasion by osteoclasts and osteoblasts, leading to osteointegration and further vascularization in bone substitute materials [Tas 2003]. Porosity also increases the surface area of the implant increasing the overall reaction speed markedly. Surface treatments such as roughening, and surface dissolution of implants in SBF or other biomimetic methods are also used to obtain a better biological response. Even crystallization has been observed to improve bone response in apatite-mullite glasses [Freeman et al. 2003]. The bioactivity of Bioglass® derived glass-ceramic was also maintained even after scaffold fabrication by sintering, which caused thorough crystallization to $Na_2Ca_2Si_3O_9$ crystals [Chen et al. 2006a]. It was shown that the crystalline phase can transform into an amorphous calcium phosphate phase after SBF treatment. The Bioglass® derived glass-ceramic scaffold can be exposed to surface functionalization, which disrupts the stable $Na_2Ca_2Si_3O_9$ crystalline phase, further enhancing the formation of the calcium phosphate phase in SBF [Chen et al. 2006b]. A positive aspect of crystallization is that the crystal phase often strengthens the glass, which was also the motive behind development of an apatite-wollastonite (A-W) glass-ceramic [Kokubo et al. 1986].

By combining glass with other materials making composite materials or structures the possibilities of implants can be widened. Composites can have a unique combination of properties of the individual components. Attempts have been made to integrate the bioactive and osteoconductive properties of bioactive glasses with bioresorbable polymers, which are easy to form. However, the interactions between bioactive glasses and polymers are not easy to predict. The presence of Bioglass® particles was found to retard the poly(lactide-co-glycolide) (PLGA) degradation rate [Boccaccini and Maquet 2003]. The same effect was found for composite scaffolds made of poly-D,L-lactide (PDLLA) and Bioglass® powder [Maquet et al. 2004]. The results also suggested that the addition of Bioglass® to polymer foams increased the water absorption and weight loss compared to plain polymer foams. The influence of

bioactive glass 13-93 in composite with PDLLA matrix to mass loss and water absorption was also reported by Niemelä et al. 2008. The degradation of the glass containing composites was lower than the degradation of the plain matrix polymer.

The degradation products of polylactides are acidic, whereas bioactive glass causes the pH to rise. However, their different degradation rates complicate any generalizations regarding the overall pH. In an *in vitro* study with a composite of bioactive glass 13-93/P(L/DL)LA, the glass dissolution increased the pH slightly at the beginning of hydrolysis, but it remained constant during weeks 2-52, suggesting that the bioactive glass neutralized the acidic degradation products of the matrix polymer [Niiranen et al. 2001]. An interesting phenomenon is related to overspill of bioactivity reactions of bioactive glasses on polymers. The extension of the calcium phosphate-rich layer originating from the bioactive glass on to adjacent polymers was called a "halo" effect, and was observed both *in vitro* and *in vivo* by Marcolongo et al. (1996, 1997). The same mechanism was harnessed to treat a partially bioresorbable glass fiber composite [Väkiparta et al. 2005]. Hydroxycarbonate apatite was formed after the biomimetic treatment. The study showed that calcium phosphate can penetrate even into the canals formed between the glass fibers and non-resorbable polymer matrix.

2.4. Thermal forming operations

The way in which the viscosity of a glass changes with temperature is a crucial factor determining which forming operations can be used in making different glass articles. Both sintering and fiber drawing processes require closely controlled viscosity.

Viscosity – a decisive factor in forming glass

Viscosity of molten glass increases gradually with decreasing temperature and approaches an infinite viscosity value as the melt solidifies. The transition from liquid to solid glass is usually associated with a specific viscosity value of 10^{13}-$10^{13.5}$ dPa·s. Glass does not have a melting point. The viscosity of liquid silicates at the liquidus temperature is several orders of magnitude larger than that of most other liquids [Kingery 1960]. In the melting furnace the viscosity of the glass melt is in the range of 10 – 10^2 dPa·s. The commercially important silicate glasses require melting temperatures of at least 1400 °C to reach this viscosity. Even then, the melting times are usually several hours in order to ensure homogeneity. A viscous melt can then be transformed to a glassy state if it fails to nucleate [Pye et al. 1972]. This can be promoted by rapid cooling called quenching.

During cooling or heating the viscosity of glasses changes strongly with the temperature. A typical viscosity-temperature curve is shown in Figure 6. A glass composition providing a steep viscosity curve is called "short". If the viscosity change is more moderate a glass is called "sweet" [Vogel 1994]. The best known and most successful representation of the variation of viscosity with temperature over a wide temperature range is a mathematical equation called the Vogel-Fulcher-Tammann (VFT) equation. Another approach is to use fixed viscosity points for the characterization of glasses. The three main fixed points are the Littleton softening point at approximately $10^{7.65}$ dPa·s, the annealing point at $10^{12\text{-}14}$ dPa·s and the strain point at $10^{14\text{-}14.5}$ dPa·s (Cable 1991). The temperatures at which these fixed viscosity points are obtained depend on the chemical composition of the glass.

Many attempts have been made to mathematically relate the dependence of viscosity on composition, one of the most notable being by Lakatos et al. (1974). These models are usually based on experimental values and are valid only for limited glass composition ranges. A problem concerning viscosity measurements is that no method alone can be used over the whole viscosity range due to its wideness [Rawson 1980]. Since viscosity is the primary property determining the temperature level at which different melt forming take place, work to predict reliable viscosity curves based on composition alone continues [Fluegel 2007]. Viscosity models would be worthwhile for optimizing glass compositions with improved working properties for particular manufacturing processes and also for knowing how sensitive a glass at issue is to any change in glass composition [Rawson 1980]. Meanwhile, some results suggesting trends in how viscosity changes are composition related have been reported. Apparently, viscosity depends on the network structure. The more ions with modifier character are involved, the more bridge rupture they are expected to cause, which is related to viscosity decrease [Kingery 1960, Rawson 1980]. Yet changes in alkali content are not expected to cause substantial effects [Rawson 1980]. Viscosity models for multicomponent systems in the range of bioactivity have been proposed by Karlsson and Rönnlöf (1998) and Vedel et al. (2008).

Sintering

Sintering is a method for making objects from powder by a spontaneous adhesion of particles during heating. The viscosity at which glass particles can adhere to each other to form a porous body is approximately 10^8 – $10^{8.8}$ dPa·s [Cable 1991, Shelby 1997]. The surfaces of the glass particles become soft and sintering through viscous flow is achieved. As a result, sharp edges on the particles become round and particles approach each other. Finally the particles are essentially glued together by neck formation between the particles and an object with a certain porosity is created. With prolonged sintering the porosity can also be eliminated entirely.

The sintering mechanism of glass is diffusion. A model to describe the early stages of sintering is known as the Frenkel model, according to which the driving force for sintering is the reduction in the free surface energy of the material, which means that the total surface area of the material diminishes. The energy released by the decrease in surface energy is used for viscous flow, which is responsible for the mass transport that produces densification. The Frenkel model has been further developed, for example by Zanotto and Prado (2001), to cover the whole sintering process. The outcome of a sintering process can be controlled, in addition to viscosity, by temperature and time together with particle size and packing degree of the sintering powder. Another reason to closely control the sintering parameters is to avoid spontaneous crystallization, which hinders viscous flow sintering and leads to residual porosity [Zanotto 2003]. Therefore, the sintering through viscous flow should be complete before crystallization occurs [Siligardi 2000]. Unfortunately, these two kinetic processes, viscous flow and crystallization, usually occur simultaneously in the same temperature range [Prado et al. 2002]. Also, a decrease in viscosity accelerates both processes.

Traditionally, a constant temperature is used for a specific time to achieve a desired sintering result. An approach that uses a constant heating rate in order to gain full densification prior to crystallization has been suggested by Boccaccini et al. (1996). In that study, heating microscopy was used for studying the interaction between

densification and crystallization. Heating microscopy techniques can also be combined with DTA to describe sintering and crystallization processes [Siligardi et al. 2000, Barbieri et al. 2003, Rawlings and Boccaccini 2004]. To be able to control the sintering process and thereby the outcome, viscosity measurements are of utmost importance and heating microscopy can also be used to determine the viscosity-temperature dependence of glasses [Eitel 1976, Scholze 1962, Karlsson and Rönnlöf 1998, Pascual et al. 2005, Vedel et al. 2008]. However, more often viscosity is determined with a rotation viscosimeter, which can be used to measure the viscosity of glass up to 10^7 dPa·s.

Porous bodies made by sintering bioactive glass microspheres have been studied *in vitro* by Ylänen et al. (2000a) and Itälä et al. (2002). Sintering enables manufacturing of porous implants of different shapes and sizes. An advantage of porosity is that it increases the total reacting surface and also allows new bone ingrowth into the implant [Ylänen et al. 2000b]. Microroughness can be created on the microspheres by etching, which significantly enhances the bone bonding response of the porous glass matrix [Itälä et al. 2001]. However, the degree of new bone formation has also been found to be dependent on the bioactive glass composition [Itälä et al. 2003]. Implants with controlled porosity can also be sintered from crushed glass. The sintering range and optimum sintering parameters depend on the chemical composition of the glasses [Fröberg et al. 2004]. The glass composition is also relevant to the crystallization tendency. For making porous implants by viscous flow sintering, only compositions tolerating thermal treatments in the sintering range without crystallization are acceptable. The working range for bioactive glasses could be enlarged by decreasing the amount of alkali oxides and by increasing the amount of alkaline earth oxides [Brink 1997].

Fiber drawing

The viscosity required for fiber formation from oxide glass melt is $10^3 - 5 \cdot 10^3$ dPa·s. This viscosity will occur at different temperatures depending on the composition. The liquidus temperature should preferentially be properly below the temperatures corresponding to fiber forming viscosities in order to provide a comfortable margin for fiber spinning or drawing. Wallenberger (2002) has extensively studied the mechanism of fiber formation. He comments: *"Viscous melts from which fibers may be spun are either strong or fragile melts. The difference in melt behaviour could be described as differences in temperature variation of viscosity in the fiber forming range and in liquidus temperature. With strong melts, fibers can be downdrawn directly from a melt or a solid preform. But fibers from fragile melts require updrawing from a supercooled melt or rapid quenching of the fibers"*. E-glass type silicate melts are usually strong, i.e. showing a straight-line rise in temperature. Thus, fiber drawing is possible by 1) conventional melt spinning through a spinneret while maintaining the melt above the liquidus, 2) down drawing from preforms where the melt is around the liquidus or 3) supercooled melt drawing [Wallenberger 1997].

A commercial glass composition that has good electrical properties and high tensile strength is commonly known as E-glass. It is also used extensively for fiber production using melt spinning techniques due to its excellent fiber forming capabilities. The viscosity curve for E-glass is shown in Figure 6. The fiber forming temperature range is approximately 1174 to 1196 C° depending on the exact composition. At this temperature the melt viscosity equals 10^3 dPa·s. The liquidus

temperature ($T_L \approx 1050C^o$) is well the below fiber forming temperature range, making it suitable for fiber production [Wallenberger et al 2004]. E-glass is used almost exclusively as the reinforcing phase in the material commonly known as fiberglass, which is used in, among other things, construction, the boat and transport industry, the blades of modern windmills and sports gear. Optimal strength properties are gained when straight, continuous fibers are aligned parallel in a single direction. To promote strength in other directions, laminate structures can be constructed, with continuous fibers aligned in other directions. Random direction mats and woven fabrics are also commonly used.

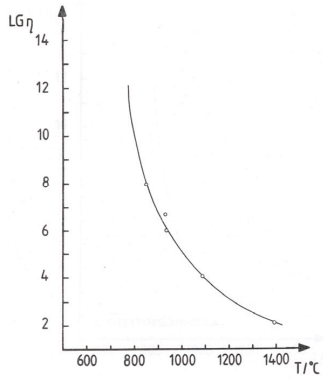

Figure 6. Viscosity-temperature curve of E-glass [Purola 1984]

The possibilities for using fibers in many ways have encouraged research groups working with bioactive glasses to produce bioactive glass fibers with promising results. Especially attractive is to combine bioactive glass fibers with polymers for osteoconducting purposes. Strong fibers with a molar composition of 30% Na_2O, 15% CaO, 3% P_2O_5 and 52% SiO_2 were soaked in SBF to verify bioactivity [Marcolongo et al. 1997]. A composite structure of these bioactive glass fibers and polysulfone achieved fixation to bone tissue through a triple mechanism consisting of bonding to the bioactive glass fiber, mechanical interlocking between the tissue and glass fibers, and close apposition and possible chemical bonding between portions of the polymer and bone tissue [Marcolongo et al. 1998]. Thick fibers (>165 μm) can also be drawn from 45S5 at 1300°C [De Diego et al. 2000]. With a composite of bioactive glass fibers (13-93) and polylactide, the flexural modulus and strength of bone tissue were reached [Pirhonen et al. 2001]. The attachment of osteoblasts was studied with fibers drawn from glasses, S520 and 45S5 [Clupper et al. 2003, 2004]. Osteoblasts remained attached after 14 days on fibers of the two glasses suggesting good bone applicability. Muscle implantation of bioactive glass fibers has also been tested but resulted in an intense inflammatory reaction [Pazzaglia et al. 1989]. However, no sign of inflammation was found in another study of bioactive glass fibers of two different compositions, namely 20-92 and 13-93, implanted in soft tissue [Brink et al. 1997b].

Knitting, weaving and other kinds of mechanical processing are demanding for bioactive fibers, which are after all fragile fibers. The traditional way to coat E-glass with silanols was applied to Bioglass® fibers in the work of Jiang et al. (2005a,b). An amine-ended silane was applied to the fiber surface and the amine groups were then used to initiate polymerization of ε-caprolactone. This improved the Young´s modulus and flexural strength of the composite, and craniofacial osteoblasts exhibited a positive response to it. Bioabsorbable polymers have also been used successfully to coat bioactive fibers, and improved the mechanical properties of the composite

drastically [Paatola et al. 2001]. As technical problems related to bioactive glass fibers are being solved, the possibilities to create new medical products are numerous. A couple of examples that have been proposed in the imaginative outlook of Karlsson (2004) are optical fibers made of bioactive glass having predetermined dissolution times, allowing post operational follow up and calcium releasing fibers for osteoporosis treatment.

3. MATERIALS AND METHODS

The experimental part of this thesis consists of determinations of physical and chemical properties of 36 multicomponent glasses. Thirty of these glasses belong to a series whose compositions were statistically chosen to cover the composition field of interest for bioactive glasses. Four well-known bioactive glasses, namely 45S5, S53P4, 13-93 and 1-98, were used as references. The motivation behind the choices of the compositions is given in Vedel et al (2008). Based on the results of the first experiments (Papers I-III) two new glass compositions, glass 16-06 and glass 17-06, were calculated and used for fiber drawing experiments as represented in Paper VII. These two compositions lie within the same compositional range as the other thirty. The compositions for all experimental glasses are given in Table 3.

Table 3. The compositions of thirty experimental glasses in the -04 series and two from -06 series given in wt-% (mole%). The reference glasses 45S5, S53P4, 13-93 and 1-98 are also included. The oxide range is valid for all glasses except for 45S5.

Glass	Na_2O		K_2O		MgO		CaO		B_2O_3		P_2O_5		SiO_2	
1-04	15	(15.4)	15	(10.1)	0	(0)	17.5	(19.8)	1	(0.9)	1	(0.4)	50.5	(53.4)
2-04	15	(14.8)	7.5	(4.9)	3	(4.5)	20	(21.8)	2	(1.8)	2	(0.9)	50.5	(51.4)
3-04	5	(4.9)	15	(9.7)	6	(9.1)	22.5	(24.5)	0	(0)	1	(0.4)	50.5	(51.3)
4-04	20	(19.4)	7.5	(4.8)	4.5	(6.7)	17.5	(18.7)	0	(0)	0	(0)	50.5	(50.4)
5-04	15	(14.7)	11.25	(7.3)	6	(9.1)	15	(16.3)	1	(0.9)	1	(0.4)	50.75	(51.4)
6-04	25	(23.6)	0	(0)	6	(8.7)	15	(15.6)	3	(2.5)	0	(0)	51	(49.6)
7-04	15	(14.1)	0	(0)	6	(8.6)	25	(25.9)	2	(1.7)	1	(0.4)	51	(49.3)
8-04	20	(19.8)	3.75	(2.4)	1.5	(2.3)	17.5	(19.2)	3	(2.6)	3	(1.3)	51.25	(52.4)
9-04	20	(19.9)	7.5	(4.9)	1.5	(2.2)	17.5	(19.2)	0	(0)	2	(0.9)	51.5	(52.8)
10-04	10	(9.7)	3.75	(2.4)	4.5	(6.7)	22.5	(24.2)	3	(2.6)	4	(1.7)	52.25	(52.5)
11-04	20	(19.9)	3.75	(2.5)	0	(0)	20	(22.0)	1	(0.9)	3	(1.3)	52.25	(53.5)
12-04	20	(19.7)	7.5	(4.8)	3	(4.5)	15	(16.3)	1	(0.9)	1	(0.4)	52.5	(53.2)
13-04	20	(19.6)	3.75	(2.4)	3	(4.5)	17.5	(18.9)	0	(0)	3	(1.3)	52.75	(53.3)
14-04	20	(19.6)	3.75	(2.4)	1.5	(2.3)	20	(21.6)	0	(0)	2	(0.9)	52.75	(53.3)
15-04	5	(5.0)	11.25	(7.3)	6	(9.2)	17.5	(19.2)	4	(3.5)	3	(1.3)	53.25	(54.5)
16-04	5	(5.0)	7.5	(4.9)	3	(4.6)	25	(27.4)	2	(1.8)	4	(1.7)	53.5	(54.7)
17-04	10	(9.5)	0	(0)	6	(8.8)	22.5	(23.7)	3	(2.6)	4	(1.7)	54.5	(53.7)
18-04	15	(14.5)	0	(0)	4.5	(6.7)	20	(21.3)	2	(1.7)	4	(1.7)	54.5	(54.2)
19-04	10	(10.0)	11.25	(7.4)	0	(0)	22.5	(24.8)	1	(0.9)	0	(0)	55.25	(56.9)
20-04	10	(10.1)	7.5	(5.0)	0	(0)	20	(22.4)	3	(2.7)	4	(1.8)	55.5	(58.0)
21-04	5	(5.0)	11.25	(7.4)	4.5	(6.9)	17.5	(19.2)	4	(3.5)	2	(0.9)	55.75	(57.2)
22-04	25	(24.5)	0	(0)	0	(0)	15	(16.2)	2	(1.7)	2	(0.9)	56	(56.6)
23-04	5	(4.9)	11.25	(7.3)	4.5	(6.8)	20	(21.7)	2	(1.8)	1	(0.4)	56.25	(57.1)
24-04	15	(15.2)	11.25	(7.5)	0	(0)	15	(16.8)	1	(0.9)	1	(0.4)	56.75	(59.2)
25-04	15	(14.6)	3.75	(2.4)	0	(0)	22.5	(24.2)	2	(1.7)	0	(0)	56.75	(57.0)
26-04	10	(9.6)	0	(0)	3	(4.4)	25	(26.5)	1	(0.9)	3	(1.3)	58	(57.4)
27-04	5	(4.8)	7.5	(4.8)	3	(4.5)	25	(26.6)	0	(0)	0	(0)	59.5	(59.3)
28-04	5	(4.9)	11.25	(7.2)	6	(9.0)	15	(16.2)	3	(2.6)	0	(0)	59.75	(60.1)
29-04	10	(9.4)	0	(0)	4.5	(6.5)	20	(20.8)	3	(2.5)	0	(0)	62.5	(60.7)
30-04	10	(9.8)	3.75	(2.4)	3	(4.5)	15	(16.3)	0	(0)	4	(1.7)	64.25	(65.2)
16-06	5	(5.1)	10.2	(6.9)	0	(0)	15	(17.0)	2	(1.8)	4	(1.8)	63.8	(67.4)
17-06	10.1	(9.6)	0.2	(0.1)	6	(8.8)	15.9	(16.8)	0.2	(0.2)	3.5	(1.5)	64.1	(63.1)
45S5	24.5	(24.4)	0	(0)	0	(0)	24.5	(27.0)	0	(0)	6	(2.6)	45	(46.1)
S53P4	23	(22.7)	0	(0)	0	(0)	20	(21.8)	0	(0)	4	(1.7)	53	(53.8)
13-93	6	(6.0)	12	(7.9)	5	(7.7)	20	(22.1)	0	(0)	4	(1.7)	53	(54.6)
1-98	6	(5.9)	11	(7.1)	5	(7.6)	22	(23.1)	1	(0.9)	2	(0.9)	53	(53.8)

3.1. Preparation of the glasses (I-VII)

The batches consist of raw materials of Ph. Eur analytical reagent grade except for SiO_2, which was 99.4% pure quartz. Strong manual shaking ensured the thorough mixing of the raw material powders. The batches were melted in Pt crucibles for 3 hours at 1360ºC, casted and then annealed at 520°C for an hour before cooling to room temperature overnight in an electric furnace. The glasses were crushed and remelted for homogeneity.

Processing of glass powder and plates (I-VI)

The glasses were crushed, milled and passed through screens to give a fraction with particles of less than 45 µm in size and stored in desiccators. Also, plates with dimensions 10×20×5 mm were cut from glass blocks with a low speed saw. The surfaces of the plates were polished with a rotating grinder under water flow and finally with ethanol. Four different polishing paper roughnesses were used, beginning with 360 and finishing with 2000 mesh.

Processing of fibers (V, VII)

The fibers were drawn either from preforms or directly from glass melts at temperatures between 950 and 1150°C depending on the glass composition. The drawing from preforms was mainly conducted at the Department of Biomedical Engineering at Tampere University of Technology (TUT). The drawing methods and temperatures used for each composition are given in Table 4. A semi-automatic laboratory scale fiber drawing process was used to manufacture continuous monofilament fibers (with diameters ranging from 25 to 150 µm). The fibers were reeled up with a motorized spinning roller. The drawing velocity adjusted the diameter of the fiber. Manual drawing of short fibers (with diameters 130-500 µm) was also used for some compositions. The fibers were stored in desiccators prior to analysis.

Table 4. Fiber drawing methods and temperatures. CF= continuous fibers drawn during a long period of time. SF = continuous fibers drawn during a short period of time. FF = fragile fibers with white appearance. Fiber drawing from preforms was conducted at TUT except for glass 26-04 (ÅA).

	PREFORM		MELT	
Glass	**Temperature range [ºC]**	**Remarks**	**Temperature range [ºC]**	**Remarks**
22-04	850-880	CF	995-1015	SF
26-04	1035	SF	1045-1065	SF
27-04	1115	SF	-	-
30-04	1065-1080	FF	1050-1055	CF
16-06	-	-	1145-1155	CF
17-06	975-1035	SF	1050-1100	CF
45S5	-	-	<1360	SF
S53P4	-	-	<1360	SF
13-93	920-960	CF	-	-
1-98	940-965	CF	1120	SF

3.2. Methods to study thermal behavior (I-VI)

Differential Thermal Analysis, DTA

Alumina crucibles were filled with 15 mg of glass powder (Ø < 45 µm). The samples were first dried in the DTA furnace by heating to 350°C and then cooling to 100°C, after which the samples were heated to 1360°C at a constant rate of 20°C/min. For activation energy measurements, different heating rates ranging from 5 to 40°C/min were used. A double crucible system consisting of platinum crucibles inside alumina crucibles was used for liquidus measurements to prevent sticking of the platinum crucible to the platinum thermocouple. Both heating and cooling curves (20°C/min) were recorded. Nitrogen was used as the purge gas. The measurements were performed with a Mettler Toledo TGA/SDTA851[e].

Hot Stage Microscopy, HSM

The glass powder (Ø < 45 µm) was also used for measurements with Hot Stage Microscopy. Samples were prepared by pressing glass powder into cylinders with a spring-loaded hand press to ensure the same pressure for each sample. The height of the cylinders was 3 mm and the diameter was 2 mm. The samples were heated to 480°C at 40°C/min and then to 1200°C at 5°C/min (up to 1350°C for liquidus measurements). Measurements were also performed according to the same heating procedure, but intentionally interrupted by quenching the samples at selected temperatures. The samples were imaged at room temperature and after every 5°C increase from 500°C. The change in the height of the sample was measured from these images. The hot stage (or optical heating microscopy system, OHM) was manufactured by Misura (Expert Systems).

Heat-treatment + X-ray diffraction analysis, XRD

Glasses were heat treated in two different ways. The glass powder (approx. 20 mg) was heated on a platinum foundation in a programmable electrical laboratory furnace with a heating rate of 20°C/min up to a chosen top temperature. When the top temperature was reached the samples were removed from the furnace and allowed to cool to room temperature in static air. The samples were ground to powder in an agate mortar for the X-ray diffraction analysis.

Glass plates were also heat treated, in a preheated tube furnace on a graphite holder. The temperature in the furnace was measured with a separate thermocouple attached to a graphite holder under the sample. The heat treatments were performed in nitrogen for different periods of time, which was calculated from the time point when the sample had reached the preset temperature. After the heat treatment the samples were allowed to cool in static air. The temperatures varied between 600 and 1000 °C.

The crystalline phases formed in the parent glasses were identified with X-ray diffraction analysis (X'pert by Philips, Cu K_α radiation).

Gradient furnace and rotational viscometer analyses

For liquidus temperature measurements some glasses were sent to the Glass Research Centre, Glafo, Sweden [Paper V]. Glasses were heat treated in platinum boats in a gradient furnace and subsequently characterized by polarized-light optical microscopy. The values indicating crystallization of the samples during viscosity measurements with a rotational viscometer were also recorded [Vedel et al. 2008].

3.3. *In vitro* testing (VI, VII)

Heat-treated glass plates

The *in vitro* bioactivity of heat-treated glass plates was tested by soaking the samples for 24, 72 and 168 h in simulated body fluid (SBF) prepared according to Kokubo et al. (1990). Also, samples cut along the length axis to give a freshly cut and polished surface were soaked in SBF. The temperature of the SBF was held at 37 °C.

Fibers

The fibers were cut into 5 cm pieces and glued together at one end to give bundles of approximately 20 fibers. The bundles were soaked in SBF at 37 °C for 2-168 hours. After soaking the bundles were embedded in epoxy resin. Cutting the bundles from the middle and polishing the surface allowed cross-sections of the samples to be visualized by SEM.

3.4 Surface analysis by Scanning Electron Microscopy, SEM (II-VII)

Crystal formation and the effect of *in vitro* testing on samples were imaged and analyzed using a scanning electron microscope equipped with an electron dispersive X-ray analyzer (FEG-SEM/EDXA, LEO 1530, Zeiss and Vantage, Thermo Electron Corporation). Prior to analysis, samples were sputtered with carbon.

4. RESULTS

4.1. Crystallization tendency (Papers I-V)

Characteristic temperatures

The crystallization tendency was studied by comparing the characteristic temperatures on the differential thermal analysis (DTA) curves for the different glass compositions. The temperatures of glass transformation ($\mathbf{T_g}$), onset of crystallization ($\mathbf{T_x}$), crystallization peak ($\mathbf{T_p}$) and liquidus ($\mathbf{T_L}$) appeared as endothermic and exothermic deviations from the baseline during DTA. $\mathbf{T_g}$ was seen as the first endothermic peak on the curve. The onset of a large exothermic peak that followed the $\mathbf{T_g}$ peak was taken as $\mathbf{T_x}$. For some glasses, a low exothermic peak was observed before the large exothermic peak. However, no evidence of crystallization could be obtained with other methods at the temperatures of the low peaks. Compatibility was observed with an "elbow" in the height curve of hot stage microscopy (HSM) indicating sintering. Glasses that showed no elbow on the sintering curve by HSM showed none or only minor sintering before crystallization. Therefore it is suggested that the exothermic peak coinciding with the elbow on the HSM curves is due to sintering. Exothermic peaks due to sintering have been observed when glaze and glass powders with fine particle sizes have been studied [Schiller 1981]. The temperatures $\mathbf{T_g}$ and $\mathbf{T_x}$ define the theoretical sintering range and were thus measured for the whole "-04" glass series as given in Table 5 [Paper II and Vedel et al. 2008]. The sintering range indicated for each glass is valid for this particular glass particle size fraction and heating rate. However, the relative tendency to sinter and crystallize can be extrapolated to other fractions and heating rates as well. According to $\mathbf{T_g}$ and $\mathbf{T_x}$ values the experimental glasses could be divided into two groups: (1) glasses with a transformation temperature around 500°C and onset of crystallization below 780°C, i. e. glasses with a narrow sintering range, and (2) glasses with a transformation temperature between 555 and 640°C and onset of crystallization around 890°C, corresponding to glasses with a wider sintering range.

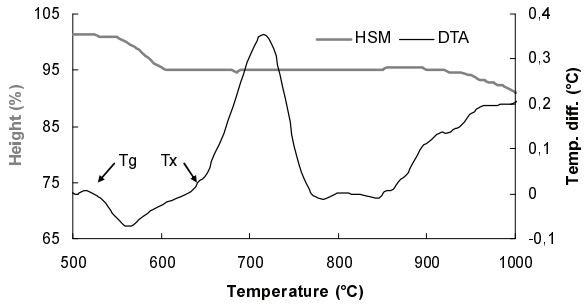

Figure 7. DTA and HSM curves recorded for glass 45S5, which has a narrow sintering range [Paper I].

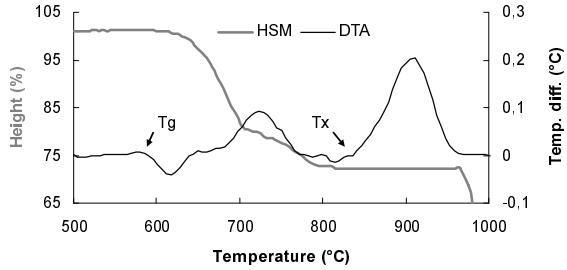

Figure 8. DTA and HSM curves recorded for glass 3-04, which has a wide sintering range [Paper I].

The division of glasses into the two groups could also be seen in the two different shapes of shrinkage graphs obtained by HSM. Examples of the two types of thermographs obtained by DTA and HSM are presented in Figures 7 and 8. HSM graphs also provided T_x, which was determined from the intercept of the horizontal plateau appearing for all the glasses (Table 5). The slight difference in the devitrification temperatures suggested by DTA and HSM is assumed to depend on the different heating rates employed in the two methods. The heating rates, 20 °C/min in DTA and 5 °C/min in HSM, were chosen to give optimal signals for each method.

Table 5. The approximate sintering range as determined by $\mathbf{T_g}$ and $\mathbf{T_x}$ values measured by DTA and HSM, showing glasses with a narrow range in the left column and those with a wide sintering range right column. **Tx**, the temperature range of crystallization, was verified by XRD from heat treated samples.

Glass	$\mathbf{T_g}$ DTA	$\mathbf{T_x}$ DTA	$\mathbf{T_x}$ HSM	$\mathbf{T_x}$ XRD	**Glass**	$\mathbf{T_g}$ DTA	$\mathbf{T_x}$ DTA	$\mathbf{T_x}$ HSM	$\mathbf{T_x}$ XRD
1-04	490	647	590	<675	3-04	590	851	790	720-880
2-04	520	699	635	<720	10-04	590	860	810	720-880
4-04	480	615	585	<620	15-04	560	905	835	>900
5-04	500	684	615	<700	16-04	610	924	850	890-950
6-04	490	624	585	<640	17-04	590	890	820	820-905
7-04	560	746	675	≈700	18-04	555	840	780	<860
8-04	510	685	615	≈635	20-04	580	870	800	<950
9-04	505	648	605	<675	21-04	560	890	845	<915
11-04	525	689	625	<700	23-04	590	910	830	740-910
12-04	480	656	580	<665	26-04	610	895	820	815-920
13-04	500	687	620	<700	27-04	640	891	845	780-890
14-04	505	673	625	<700	28-04	570	923	850	750-940
19-04	560	774	675	700-790	29-04	600	884	810	740-895
22-04	500	689	625	<710	30-04	590	900	875	<915
24-04	505	729	700	≈700	*16-06*	*532*	*940*	*880*	*>1010*
25-04	560	768	675	700-780	*17-06*	*600*	*950*	*910*	*<880*
45S5	530	647	600	<680	**13-93**	600	853	825	710-910
S53P4	541	693	645	<700	**1-98**	600	880	805	740-895

All the measured values (except values for the four reference glasses, and glasses 16-06 and 17-06) were subjected to multiple regression analysis using the backward elimination procedure. The dependence of $\mathbf{T_g}$ and $\mathbf{T_x}$ values on composition are given by equations 1-3 [Paper II].

$$Tg_{DTA}(°C) = -122.85 + 2.59 \cdot x_{K_2O} + 5.36 \cdot x_{MgO} + 9.37 \cdot x_{CaO} + 4.08 \cdot x_{B_2O_3} + 6.45 \cdot x_{P_2O_5} + 8.04 \cdot x_{SiO_2} \quad (1)$$

R^2=95.85 d.f. = 23, significance level 95%

$$Tx_{DTA}(°C) = 191.70 - 9.51 \cdot x_{Na_2O} + 5.91 \cdot x_{MgO} + 5.93 \cdot x_{CaO} + 15.29 \cdot x_{B_2O_3} + 12.92 \cdot x_{P_2O_5} + 9.77 \cdot x_{SiO_2} \quad (2)$$

R^2=96.34 d.f. = 23, significance level 95%

$$Tx_{HSM}(°C) = 182.98 - 9.60 \cdot x_{Na_2O} + 8.01 \cdot x_{MgO} + 8.52 \cdot x_{B_2O_3} + 21.98 \cdot x_{P_2O_5} + 10.69 \cdot x_{SiO_2} \quad (3)$$

R^2=95.81 d.f. = 24, significance level 95%

Seven compositions were chosen for studying in detail the factors affecting crystallization of bioactive glasses (Paper III). For this purpose also the crystallization peaks ($\mathbf{T_p}$) and liquidus temperatures ($\mathbf{T_L}$) were also determined from DTA thermographs and used together with $\mathbf{T_g}$ and $\mathbf{T_x}$ to calculate glass stability values (Table 6). Glass stability is presented as the Hruby parameter $\mathbf{K_{gl}}$ and reduced glass transition value $\mathbf{T_{RG}}$ [Hruby 1972, Turnbull 1965]. The equations for calculating these values are given below.

$$K_{gl} = \frac{T_x - T_g}{T_l - T_p} \qquad T_{RG} = \frac{T_g}{T_l}$$

Glasses having high $\mathbf{T_x}$ values also showed higher $\mathbf{K_{gl}}$ values, indicating higher stability against crystallization [Cabral et al. 1997]. These glasses were also more stable against crystallization according to the $\mathbf{T_{RG}}$ values. In fact, glasses 10-04, 23-04, 29-04 and 1-98 had $\mathbf{T_{RG}}$ values higher than 0.58, which has been reported as the limiting value for internal nucleation [James 1985]. Glasses 45S5, 7-04 and 22-04 had $\mathbf{T_{RG}}$ values below 0.58, indicating internal nucleation. Although both stability parameters gave similar trends, the $\mathbf{K_{gl}}$ was likely to describe the stability of bioactive glasses better as it also takes into account the crystallization temperature of the glass.

Inverse crystallization peak values ($\mathbf{100/T_p}$) at different heating rates were used to draw lines for the determination of activation energy for crystallization, $\mathbf{\Delta E}$, as given in Figure 9. These values were needed for Avrami constant **n** calculations using the equation below [Augis and Bennett 1978].

$$n = \frac{2.5}{\Delta\tau_{FWHM}} \frac{T_p^{\,2}}{\Delta E / R}$$

$\Delta\tau_{FWHM}$ is the full width at half maximum of the DTA peak, as seen in Figure 10.

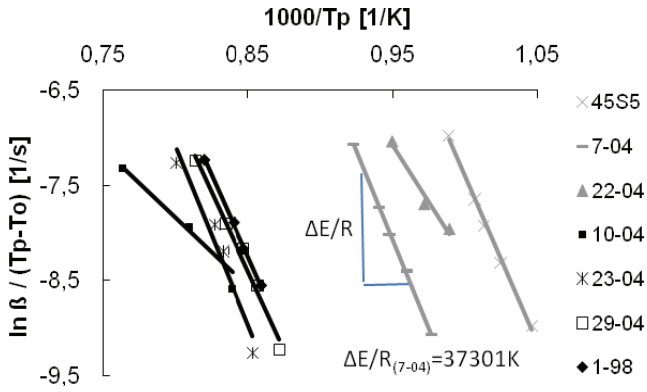

Figure 9. Determination of the ΔE/R using the Modified Kissinger method.

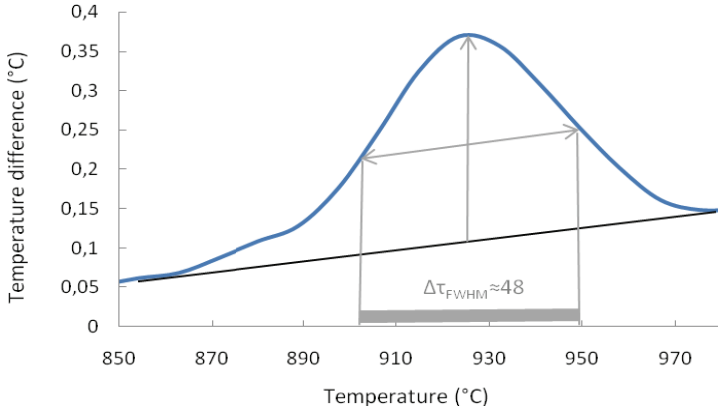

Figure 10. Determination of $\Delta\tau_{FWHM}$ from a DTA crystallization peak.

Table 6. Temperatures (°C) of glass transformation ($\mathbf{T_g}$), onset of crystallization ($\mathbf{T_x}$), crystallization peak ($\mathbf{T_p}$) and liquidus ($\mathbf{T_L}$) obtained from DTA (heating rate 15°C/min) as well as the calculated glass stability values, $\mathbf{K_{gl}}$ and $\mathbf{T_{RG}}$ together with activation energy for crystal growth **ΔE** given as kJ mol $^{-1}$ and the Avrami constant **n** [Paper III]. (Abbreviations: i = internal nucleation; s = surface crystallization).

Glass	T_g	T_x	T_p	T_L	K_{gl}	T_{RG}	ΔE	n
45S5	532	655	708	1180	0.26	0.55 (i)	293	1.06 (s)
7-04	512	747	768	1130	0.65	0.56 (i)	310	2.13 (s)
22-04	469	676	728	1130	0.51	0.53 (i)	197	1.54 (s)
10-04	570	910	943	1160	1.57	0.59	122	2.58 (s)
23-04	590	916	953	1120	1.95	0.62	311	2.41 (s)
29-04	580	892	940	1160	1.42	0.60	277	1.75 (s)
1-98	590	910	954	1100	2.19	0.63	281	1.38 (s)

The activation energies determined are in the same temperature range as values from other authors (Table 6). The activation energy for crystallization of $Na_2O{\cdot}2CaO{\cdot}3SiO_2$ crystals was reported to be 370 ± 15 kJ/mol by Xu et al. (1991) or 350 kJ/mol by Clupper and Hench (2003). Activation energy for crystal nucleation and growth of wollastonite crystals was determined by Likitvanichkul and LaCourse (1998) and was similar, at 374 kJ/mol. These crystal types were found to be formed in the experimental glasses as a result of thermal treatments, as explained in the following chapter.

The calculated Avrami constants for the experimental glasses are also listed in Table 6. These values are all below 3, suggesting that surface crystallization is dominant in all the experimental glasses, as well as for glasses 45S5, 7-04 and 22-04. This was assumed to depend on the small particle size used to measure the different peak characteristics. In systems with bulk crystallization, small particles have been reported to none the less give surface crystallization [Xu et al. 1991]. The same authors have also suggested that the crystallization mechanism of $Na_2O{\cdot}2CaO{\cdot}3SiO_2$ changes from predominantly surface to bulk due to different particle size, explaining why **n** values for glasses 45S5, 7-04 and 22-04 are below 3 and suggest surface crystallization.

The results obtained by studying these seven experimental glasses suggested that the crystallization tendency is conveniently measured by the glass stability values $\mathbf{K_{gl}}$ or $\mathbf{T_{RG}}$ while the Avrami constant **n** is likely to give reliable values only for systems consisting of large particles. However, although the activation energy for crystal growth measured from powdered glass was similar to that suggested by other authors, no clear differences between crystal type or crystallization mechanism were found when measured using this method.

Crystal formation

The reason for obtaining two types of thermographs was studied by heat-treating powdered samples and analyzing the samples by XRD. The maximum temperatures for the heat treatments were chosen according to T_x value (± 40 °C) obtained with DTA. The temperatures at which heat-treated samples gave peaks on the XRD graphs indicating crystallization are listed in Table 5. The formation of two different primary crystalline phases was observed. Glasses that crystallized at lower temperatures (615-775°C) formed sodium-calcium-silicate crystals (NCS). The exact composition of NCS crystals remained unclear, but a composition of $Na_2O{\cdot}2CaO{\cdot}3SiO_2$ was most frequently suggested, as shown in figure 11.

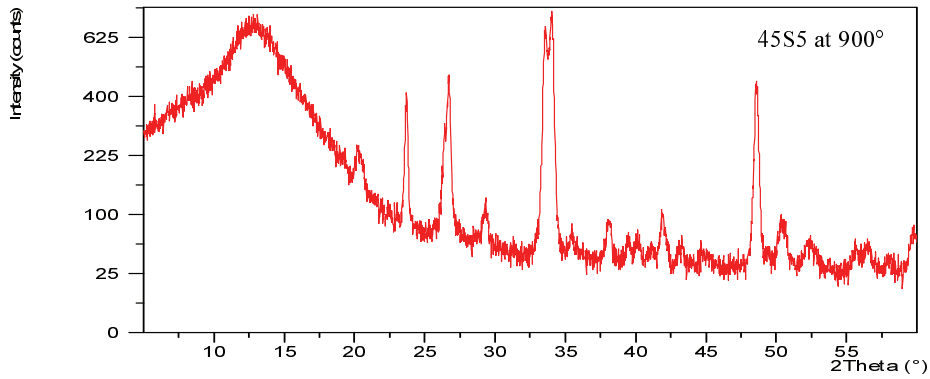

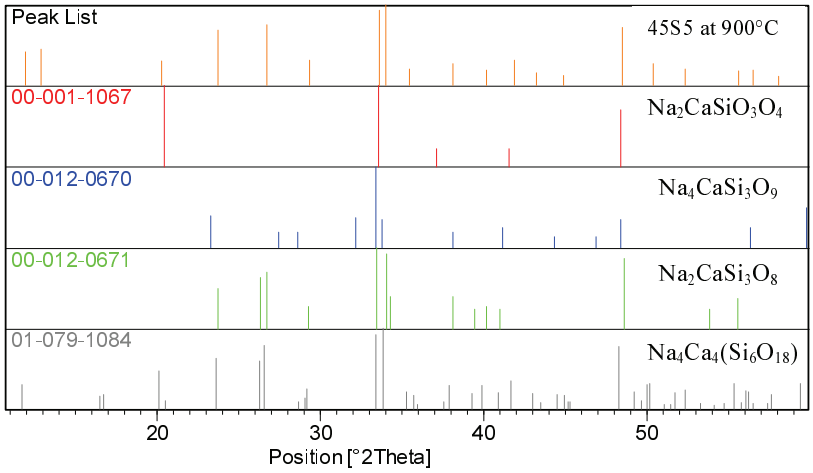

Figure 11. XRD graph of glass 45S5 heat treated at 900°C (above) and analysis of the crystal structure formed showing different possible formulas for the sodium calcium silicate (below).

Surface crystallization of β-wollastonite ($CaSiO_3$) was detected on glasses that crystallized at higher temperatures (840-950°C). In fact, heat treatments were also performed at lower temperatures on these glasses, followed by analyses with XRD, in order to confirm the absence of crystal phases at lower temperatures. The XRD patterns of heat treated samples are shown in Figure 12. For the same reason, samples from intentionally interrupted HSM measurements were imaged with SEM to understand in detail the effects of the thermal treatments, as seen in Figure 13.

Diopside was identified in some of the magnesium-containing glasses, depending on the parameters of the heat treatment. Interestingly, diopside was not observed as the primary phase in any of the glasses but appeared only after some intensive crystallization of wollastonite or sodium calcium silicate. Therefore, it was not considered to be a significant crystalline phase. A model based on the primary phases of sodium calcium silicate and wollastonite crystals was calculated. The NCS-type glasses were assigned the number 1 and the number 2 was assigned to CS glasses. Equation 4 gives the influence of oxide content on the primary crystalline phase (PCT).

$$PCT = 0.018 - 0.107\, x_{Na_2O} + 0.002\, x^2_{Na_2O} + 0.052\, x_{MgO} + 0.032\, x^2_{P_2O_5} + 0.038\, x_{SiO_2} \quad (4)$$

R^2=90.80 d.f.= 23, significance level 95%

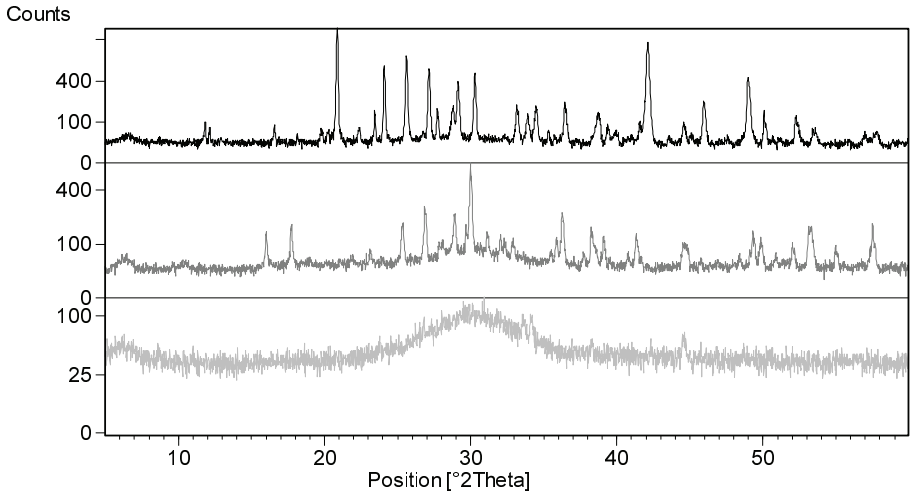

Figure 12. XRD graphs of Glass 03-04 heat treated at 720 ºC (light grey, no crystals identified), 880 ºC (dark grey, typical wollastonite pattern) and 905 ºC (black, showing primarily wollastonite formation).

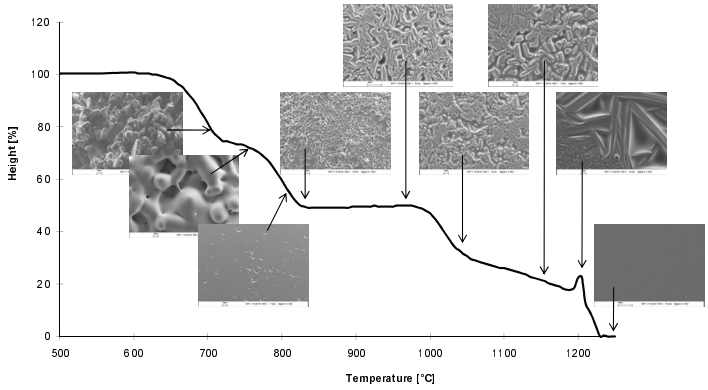

Figure 13. HSM height curve of glass 1-98 and SEM images of samples from the intentionally interrupted HSM measurements showing the growth of wollastonite crystals as a function of temperature. The magnification is the same in all the images.

The influence of heat treatment on crystallization was studied in detail for three glass compositions (Paper IV). Two of the glasses were chosen to represent formation of both crystal types, namely NCS and CS, and in addition a glass which formed NCS,

diopside ($MgCaSi_2O_6$) or wollastonite, depending on the temperature, was studied. Crystal formation in plates of these glasses was analyzed both with XRD and SEM after heat-treatments, as shown in Figure 14. NCS crystal formed at 600 °C on the surface of glass 45S5, but at higher temperatures homogenous volume crystallization was observed. On glass 1-98, crystals also formed on the surface around 800 °C, but the wollastonite crystals only grew in size inwards from the surface as time and temperature increased during the heat treatment. Glass 07-04 resisted crystallization up to 700 °C, but then crystallized with NCS as the primary crystalline phase. With increasing temperature, wollastonite and diopside formed simultaneously with sodium-calcium-silicate for glass 07-04, and at the highest temperatures the main crystalline type on the surface was diopside.

Thermal phenomena around anticipated liquidus temperature and crystallization of the glasses were characterized by several approaches, which are summarized in Table 7. Optical microscopy of the samples heat treated in the gradient furnace gave liquidus between 1125 and 1255°C depending on the glass composition. DTA gave a broad endothermic effect for most of the glasses as shown by glasses 45S5 and 1-98 in Figure 15. As the offset of the peak was equivalent to beginning of the exothermic peak on the cooling curve, the offset was used to give liquidus. These values were also in good agreement with the values obtained with the gradient furnace. Additionally, the temperatures when HSM samples had totally collapsed and smoothed out on the surface were of the same temperature range. These values are listed as HSM offset in Table 7. The temperature values of which viscosity measurement with rotational viscometer was interrupted by crystallization are also given in Table 7. This temperature value gives only a rough estimation of the liquidus temperature. The viscosity values given by the rotational viscometer were several magnitudes lower than typical viscosities which can be measured with this method. However, crystallization might have commenced already at higher temperatures.

Table 7. Temperatures (°C) describing thermal phenomena of the experimental glasses with different methods. (-) not measured, (no value) could not be identified due to minor crystallization [Paper V].

Method→	Gradient furnace	DTA onset	DTA offset	HSM onset	HSM offset	Rotational viscometer
Glass↓	Liquidus		Liquidus		Liquidus	Liquidus
7-04	1255	1010	1230	1075	1175	1135
10-04	1210	1050	1240	1040	1200	1110
17-04	1205	1070	1200	1050	1180	979
22-04	1125	1040	1180	885	1180	1105
26-04	1245	1070	1230	1080	1200	1037
30-04	-	1060	1220	1005	1275	1042
16-06	-	910	1050	no value	1300	-
17-06	-	910	1010	1060	1255	-
45S5	1210	1160	1260	1170	1270	1293
S53P4	1188	1070	1230	1035	1220	1190
13-93	-	870	1020	1050	1200	920
1-98	1235	1070	1240	1000	1225	1168

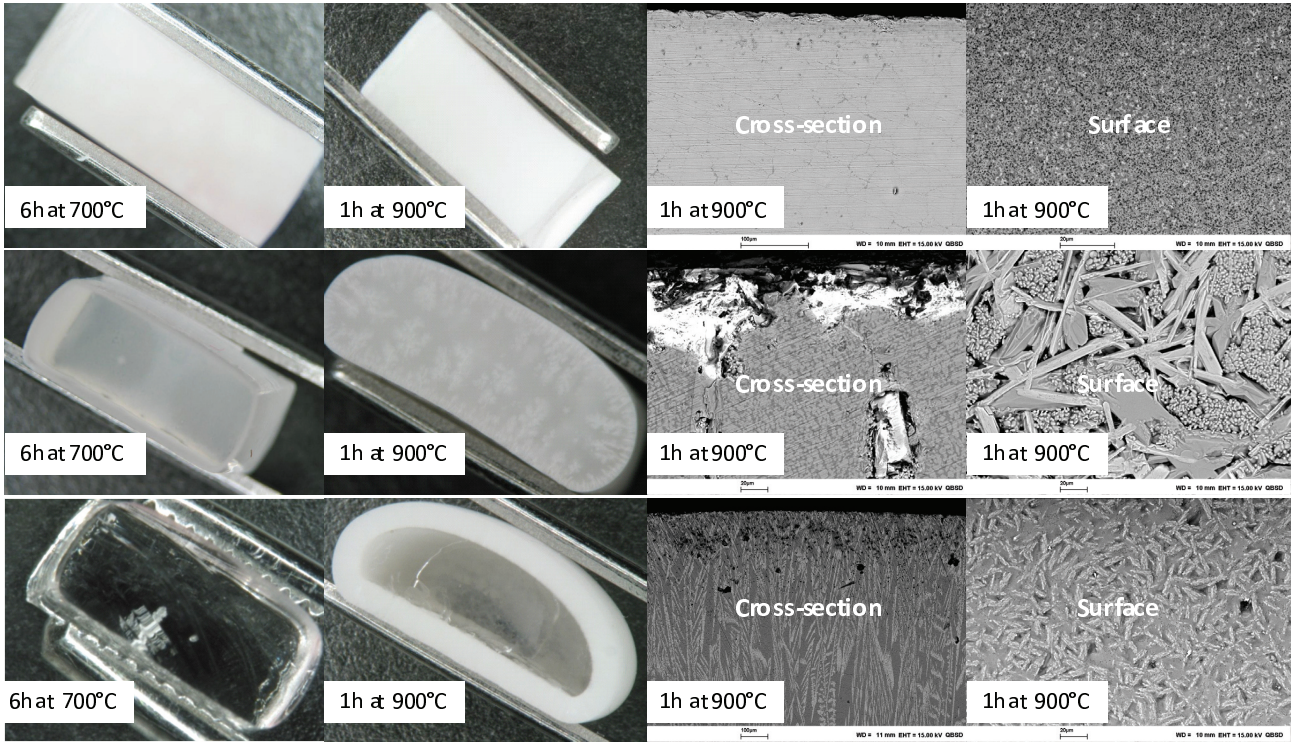

Figure 14. Heat treated glass plates of glasses 45S5 (upper row), 07-04 (middle row) and 1-98 (lowest row) imaged with a digital camera.

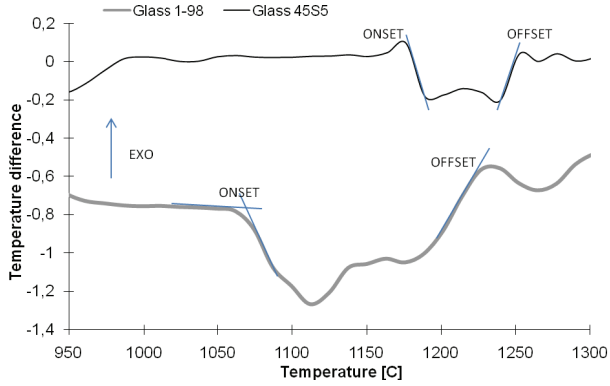

Figure 15. Heating curves of 45S5 and 1-98 obtained with DTA [Paper V].

4.2. *In vitro* bioactivity (Papers VI, VII)

The effect of crystallization on bioactivity

Bioactivity of the glasses *in vitro* was studied by soaking samples in SBF and analyzing formation of silica-rich and calcium phosphate-rich layers with SEM. After heat treatments the plates had partially crystallized, but also contained residual glass phase. The influence of sodium calcium silicate crystals on *in vitro* bioactivity was studied further with parent glasses 45S5 and 7-04. The results indicated that calcium and phosphorous precipitated both on the silica gel formed on the residual glassy phase and on the nano-sized sodium calcium silicate crystals on the sample surfaces. In glasses with a crystallized wollastonite surface layer, the corroding effect of SBF was seen with longer soaking times. SEM images of the surface of glass 1-98 heat treated for 1 h at 800°C and then soaked in the SBF for 24 and 72 hours are shown in Figure 16. The glassy phase between the wollastonite crystals formed a thin silica layer primarily by the alkalis dissolving into SBF. With longer immersion, the wollastonite crystals also started to dissolve and calcium phosphate nucleated on the silica. After prolonged immersion the surface was covered with a calcium phosphate layer. In both cases, the formation of silica-rich and calcium phosphate-rich layers indicating bioactivity, was retarded compared to untreated non-crystalline glass plates.

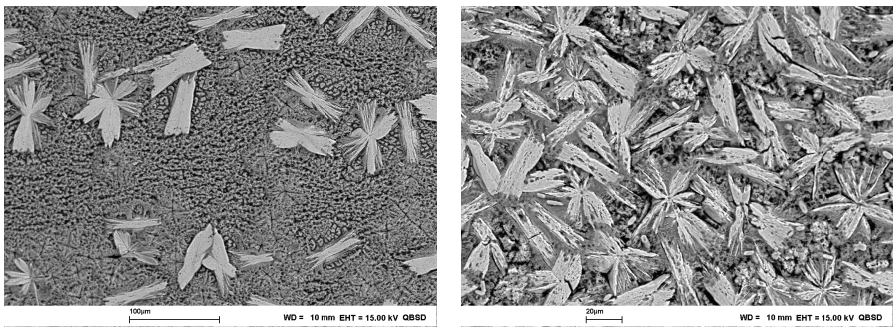

Figure 16. SEM images of glass 1-98 heat treated at 800°C for one hour and soaked in SBF for 24 hours (left) and 72 hours (right).

The bioactivity of the fibers

The fibers were also soaked in SBF to study their reactivity. The SEM analysis of cross-sections revealed three distinct, different reaction types, as shown in Figure 17. Fast-reacting fibers formed distinct silica–rich and calcium phosphate–rich reaction layers. Fibers of glasses with medium bioactivity showed formation of a thin calcium phosphate–rich layer but no clear silica-rich layer could be observed. For the third type only sporadic deposits of calcium phosphate were found on fiber surfaces touching each other.

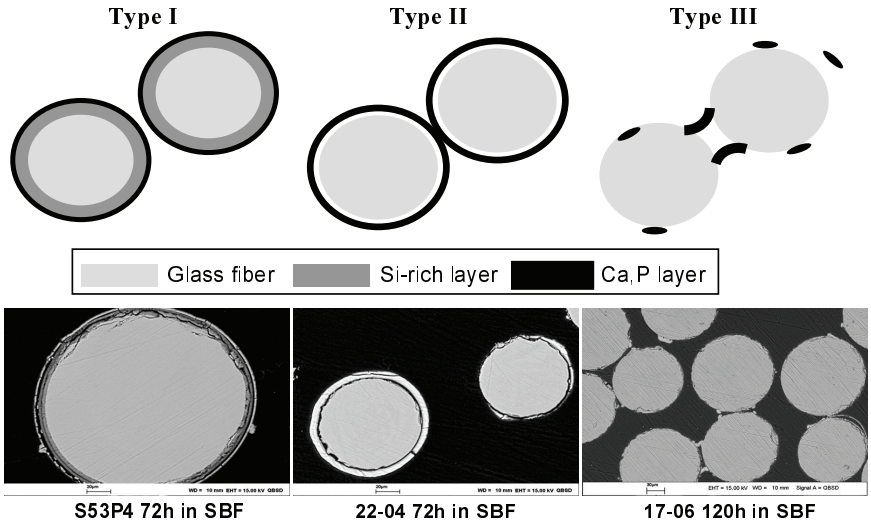

Figure 17. Sketches (above) and SEM images (below) of cross-sections of fibers showing the formation of reaction layers and precipitations according to reaction types I (rapid bioactivity), II (medium bioactivity) and III (slow bioactivity).

5. DISCUSSION

The primary crystalline phase in crystallization was found to correlate strongly with the oxide content of the glass. Glasses with a high content of alkali oxides crystallized easily to sodium calcium silicate crystals, while glasses with a high content of alkaline earth oxides gave rise to wollastonite formation. Interestingly, glass compositions which corresponded to $Na_2O{\cdot}2CaO{\cdot}3SiO_2$ rather than to $CaO{\cdot}SiO_2$ still formed wollastonite as the primary crystalline phase. Only when the molar ratio of alkalis to alkaline earths was clearly higher than 1:2 were sodium calcium silicate crystals found, as shown in Figure 18. The excess of sodium oxides seemed to be the driving force for $Na_2O{\cdot}2CaO{\cdot}3SiO_2$ crystallization. Because the primary crystals formed on the heat treated glasses were not compositionally identical to the parent glasses, other crystalline phases could still form at higher temperatures.

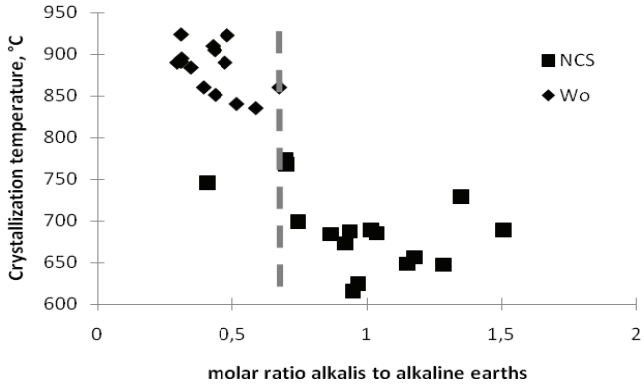

Figure 18. Crystallization temperature according to thermal analysis as a function of molar ratio of alkalis to alkaline earths. The primary phases in crystallization are $Na_2O{\cdot}2CaO{\cdot}3SiO_2$ (NCS) and $CaO{\cdot}SiO_2$ (Wo).

The classical ternary phase diagram for commercial soda-lime glasses also includes the crystalline phases $Na_2O{\cdot}2CaO{\cdot}3SiO_2$ and $CaO{\cdot}SiO_2$ [Levin et al. 1964]. By superimposing the experimental compositions on the diagram, a relatively good match of the primary fields in crystallization could be seen as shown in Figure 19. The magnesium oxide was combined with lime and potassium oxide into sodium oxide and the glass-forming oxides B_2O_3 and P_2O_5 into silica on a wt-% basis. If the effect of MgO on diopside formation is excluded, the diagram suggests that the experimental glasses belong to the sodium-calcium fields of NC_2S_3 ($Na_2O{\cdot}2CaO{\cdot}3SiO_2$) and α or β-CS ($CaO{\cdot}SiO_2$). However, the results showed that glasses having high MgO content and an alkali-glass former ratio near the boundary of the two main phases were able to form NC_2S_3, CS or diopside depending on the temperature.

The correlation of primary crystalline phase to composition could also be expressed by means of a mathematical model. Mathematical modelling provides a good tool to understand the correlation between composition and thermal behaviour, especially when complex multicomponent systems are considered. The problem with models is that they are often valid only for a certain compositional range and provided that all the experimental conditions are identical. Still, they can be used to predict approximate behavior of unfamiliar compositions and aid in further development of more customized compositions for special applications.

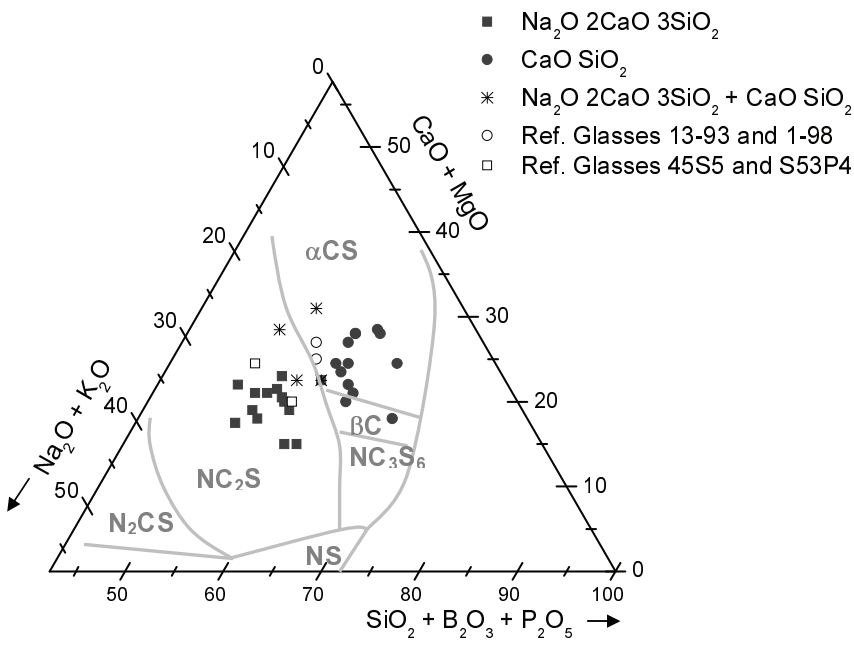

Figure 19. Primary phases at crystallization of the experimental glasses superimposed on the ternary Na_2O-CaO-SiO_2 system [Paper II].

Due to the formation of two main primary crystalline phases, the sintering range for the experimental glasses could also be divided into two types of ranges. The glasses which crystallized with NCS as the primary crystalline phase had a narrow sintering range (480-780°C). Concurrent internal nucleation leading to bulk crystallization before reaching the optimal viscosity inhibited viscous flow sintering for these glasses. A broad sintering range (550-930°C) was typical for the glasses that formed $CaSiO_3$ crystals during crystallization. They had higher stability against crystallization, which commenced first at temperatures high enough to allow sintering into porous implants prior to crystallization. A typical porous sintered implant can be seen in Figure 20.

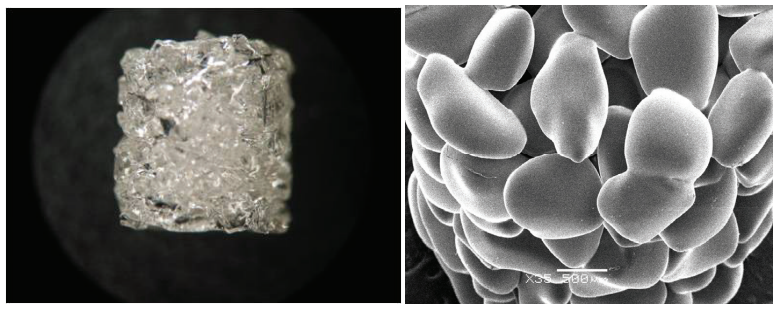

Figure 20. A sintered implant (3×5 mm) imaged with a digital camera (left) and SEM (right). The crushed glass fraction used was 300-500 µm.

The fiber drawing viscosity range coincided with the crystallization and liquidus temperatures for the glasses showing NCS formation. However, glasses showing wollastonite formation could be hot worked to some extent without excessive crystallization. Crystallization characteristics, expressed as the reduced glass transformation value and the Avrami constant, suggested that surface crystallization was the main mode of phase separation in wollastonite-type glasses. This was verified by customized heat-treatments. Therefore fiber drawing from preforms below the liquidus temperature is possible only up to the point at which crystallization begins to interfere with the drawing process. Liquidus temperatures for some wollastonite glasses indicated that fiber drawing from melt should be possible.

In vitro bioactivity was found to be affected by crystallization. Formation of silica-rich and calcium phosphate-rich layers, indicating bioactivity, was slower on surfaces of samples that included sodium calcium silicate crystals than on the parent glass. On wollastonite-forming glasses, the retarding effect of crystallization on bioactivity was also seen, but the mechanism was different. Layer formation was initiated by dissolution of the alkali from the glassy phase between crystals, leaving a thin silica layer outermost. With prolonged soaking, hydroxyapatite nucleated on the silica layer and the wollastonite crystals also started to corrode. Finally, the whole surface was covered with hydroxyapatite.

The dissolution of the thin fibers was very rapid. The reactivity of the fibers followed the same trends as the *in vitro* bioactivity of glass plates [Zhang et al. 2005]. Glasses which were classified as fast reacting in studies with glass plates were found to also react rapidly as fibers. Similarly, glasses with inefficient layer formation on plates did not create clear layers on fibers either. Also, the fibers seemed to provoke special reaction mechanisms as shown on cross-sections of the fibers. In fact, the cross-sections provided an interesting approach to investigating reaction layer formation.

The *in vitro* observations suggested that the mechanical strength of fibers with high or moderate bioactivity was rapidly lost due to dissolution mechanisms. Thus, fibers with a slow bioactivity would be suitable for applications where these fibers are used to increase the strength of composites and also to induce some bone growth.

6. CONCLUSIONS

Crystallization tendency was found to be high for all glasses which had compositions within the range of bioactivity. The main factor affecting crystallization tendency was the alkali oxide content, according to which two distinct crystallization paths were observed, leading to two different primary crystalline phases. The formation of sodium calcium silicate crystals was dominant in high alkali-content glasses and occurred slightly above the glass transition temperature. Glasses with low alkali content resisted crystallization up to 900ºC, when calcium silicate crystals were formed. However, even a minor change in glass composition had significant effects on thermal behavior. This was observed when the measured characteristic temperatures were used to model the primary crystalline phase in crystallization, together with glass transition and crystallization temperatures. Crystallization was also confirmed to have a retarding effect on *in vitro* bioactivity.

In special products made from bioactive glass, such as sintered porous bodies or continuous fibers, the oxide glass composition should be adjusted to allow desired bioactivity but also provide suitable hot working properties without any interference by crystallization, which might hinder these forming processes and influence bioactivity. The sintering range was wide enough for production of e.g. sintered porous implants, only for glasses showing calcium silicate crystal formation. These types of glasses were also preferred for fiber drawing, especially if downdrawing from preforms was used. Those glasses in which calcium silicate crystals formed as a result of surface nucleation also showed lower bioactivity *in vitro* than glasses in which sodium calcium silicate crystals were found. Fibers of low bioactivity were assumed to be suitable for composites where they would be used to reinforce the mechanical properties. If continuous fibers are desired, compositions having liquidus below fiber forming temperatures should be chosen.

The fibers produced showed *in vitro* behavior comparable to that of their equivalents in other forms such as plates. Reaction layers were observed on fibers which were expected to show bioactivity according to their composition. At best, glass fibers showing bioactivity may provide both good bone bonding characteristics and new structural possibilities for implant development, especially when combined with biodegradable polymers. However, the fragility and high dissolution rate of the bioactive glass fibers might limit their use. The models describing the crystallization temperature and the primary phase in crystallization as functions of the oxide composition of the glass can be used to tailor the glass composition according to the requirements of the applications of the bioactive glass. By tailoring the glass composition according to the requirements of the application, some manufacturing and forming obstacles can be overcome.

REFERENCES

Andersson, Ö. H., Karlsson, K. H., Kangasniemi, K. and Yli-Urpo, A., Models for physical properties and bioactivity of phosphate opal glasses, Glastechnische Berichte **1988**, 61(10), 300-5.

Andersson, Ö. H. and Karlsson, K. H., Development of bioactive glasses and glass-ceramics, in CRC handbook of Bioactive Implants, Ed. Yamamuro, T., Wilson-Hench, J. and Hench, L., CRC Press, Inc, **1990**a.

Andersson, Ö. H., Liu, G., Karlsson, K. H., Niemi, L., Miettinen, J. and Juhanoja, J., In vivo behavior of glasses in the SiO_2 - Na_2O - CaO - P_2O_5 - Al_2O_3 - B_2O_3 system, J. Mater. Sci: Mater in Med., **1990**b, 1(4), 219-27.

Andersson, Ö. H., Karlsson, K. H. and Kangasniemi, K. A., Calcium phosphate formation at the surface of bioactive glass in vivo, J. Non-Cryst. Solids, **1990**c, 119(3), 290-6.

Augis, J. A. and Bennett, J. E., Calculation of the Avrami parameters for heterogeneous solid state reactions using a modification of the Kissinger method, J. Thermal Anal., **1978**, 13, 283-292.

Backman, R., Cable, M., Karlsson, K. and Pennington, N., Prediction of liquidus temperatures in multi-component silicates, Report on EURAM project MA1E/0009/C, **1990**.

Backman, R., Karlsson, K., Cable, M. and Pennington, N., Model for liquidus temperature of multi-component silicate glasses, Phys. Chem. Glasses, **1997**, 38(3), 103-9.

Barbieri, L., Corradi, A., Lancellotti, I., Pellacani, G.C. and Boccaccini, A. R., Sintering and crystallization behaviour of glass frits made from silicate wastes, Glass Technol., **2003**, 44(5), 184-90.

Birnie, D. P. III and Weinberg, M. C., Development of anisotropic particle morphology in an isotropically transforming matrix, Physica A: Statistical Mechanics and Its Applications, **2000**, 285(3-4), 279-294.

Boccaccini, A. R. and Maquet, V., Bioresorbable and bioactive polymer/Bioglass® composites with tailored pore structure for tissue engineering applications, Comp. Sci. Tech. **2003**, 63, 2417-2429.

Branda, F., Buri, A., Marotta, A. and Saiello, S., Devitrification behaviour of glasses near the Na_2O-$2SiO_2$ composition, Thermochimica Acta, **1984**, 80, 269-274.

Brink, M., The influence of alkali and alkaline earths on the working range for bioactive glasses, J. Biomed. Mater. Sci, **1997**, 36, 109-117.

Brink, M., Laine, P., Narva, K and Yli-Urpo, A., Implantation of bioactive and inert glass fibres in rats – soft tissue response and short-term reactions of the glass, Bioceramics, **1997**a, 10, 61-64.

Brink, M., Turunen, T., Happonen, R.-P. and Yli-Urpo, A., Compositional dependence of bioactivity of glasses in the system Na_2O – K_2O- MgO-CaO - B_2O_3 - P_2O_5 - SiO_2, J. Biomed. Mater. Res., **1997**b, 37, 114-121.

Cable, M., Classical Glass Technology, in Materials Science and Technology, Vol 9., vol. ed. Zarzycki, J., VCH Publishers Inc., **1991,** ISBN: 3-527-26822-7.

Cabral, A. A. Jr., Fredericci, C. and Zanotto, E. D., A test of the Hruby parameter to estimate glass-forming ability, J. Non-Cryst. Solids, **1997**, 219, 182-186.

Chatzistavrou, X., Kontonasaki, E., Chrissafis, K., Zorba, T., Koidis, P. and Paraskevopoulos, K.M., Surface and Bulk Contributions in the Crystallization Process of a Bioactive Glass, Key Eng. Mat. **2006**, 309-311, 313-316.

Chen, Q. Z., Thompson, I. D. and Boccaccini, A. R., 45S5 Bioglass® -derived glass-ceramic scaffolds for bone tissue engineering, Biomaterials, **2006**a, 27, 2414-2425.

Chen, Q. Z., Rezwan, K., Armitage, D., Nazhat, S.N. and Boccaccini, A. R., The surface functionalization of 45S5 Bioglass® -based glass-ceramic scaffolds and its impact on bioactivity, J. Mater. Sci: Mater Med, **2006**b, 17, 979-987.

Clifford, A., Hill, R., Rafferty, A., Mooney, P., Wood, D., Samuneva, B. and Matsuya, S., The influence of calcium to phosphate ratio on the nucleation and crystallization of apatite glass-ceramics, J. Mater. Sci: Mater Med., **2001**, 12, 461-469.

Clupper, D. C., and Hench, L. L., Crystallization kinetics of tape cast bioactive glass 45S5, J. Non-Cryst. Solids, **2003**, 318, 43-48.

Clupper, D. C., Gough, J. E., Hall, M. M., Clare, A. G., LaCourse, W. C. and Hench, L. L., In vitro bioactivity of S520 glass fibers and initial assessment of osteoblast attachment, J. Biomed. Mater. Res. Part A, **2003**, 67A, 1, 285-294.

Clupper, D. C., Gough, J. E., Embanga, P. M., Notingher, I., Hench, L. L. and Hall, M. M., Bioactive evaluation of 45S5 bioactive glass fibers and preliminary study of human osteoblast attachment, J. Mater. Sci: Mater Med., **2004**, 15(7), 803-808.

Davison, S., Conservation and Restoration of Glass, second ed., by Elsevier, **2003**, ISBN: 978-0-7506-4341-2.

De Diego, M., Coleman, N. J.and Hench, L.L., Tensile properties of bioactive fibers for tissue engineering applications, J. Biomed. Mater. Res. **2000**, 53(3), 199-203.

Dietzel, A., The cation field strengths and their relation to devitrification processes, to compound formation and to the melting points of silicates, Z. Elektrochem, **1942**, 48, 9-23.

Drexhage, M. G., El-Bayoumi, O. H. and Lipson, H., Comparative study of BaF_2/ThF_4 glasses containing YF_3, YbF_3 and LuF_3, J. Non-Cryst. Solids, **1983**, 56, 51-6.

Eitel, W., Silicate Science, Vol VII Glass Science by Academic Press, Inc, **1976**, ISBN: 0-12-236307-8.

Elgayar, I., Aliev, A. E. Boccaccini, A. R. and Hill, R. G. Structural analysis of bioactive glasses, J. Non-Cryst. Solids, **2005**, 351, 173-183.

El-Ghannam, A., Hamazawy, E. Yehia, A., Effect of thermal treatment on bioactive glass microstructure, corrosion behavior, zeta-potential, and protein adsorption, J. Biomed. Mater. Res., **2001**, 55, 387-395.

Filho, O. P., LaTorre, G. P. and L. L. Hench, Effect of crystallization on apatite-layer formation of bioactive glass 45S5, J. Biomed. Mater. Res. **1996**, 30, 509-514.

Fluegel, A. Glass viscosity calculation based on a global statistical modelling approach, Glass Technol, **2007**, 48(1), 13-30.

Fokin, V.M., Zanotto, E. D. and Schmelzer, J. W. P., Homogeneous nucleation versus glass transition temperature of silicate glasses, J. Non-Cryst. Solids, **2003**, 321, 52-65.

Fokin, V. M., Nascimento, M. L. F. And Zanotto, E. D., Correlation between maximum crystal growth rate and glass transition temperature of silicate glasses, J. Non-Cryst. Solids, **2005**, 351, 789-794.

Freeman, C. O., Brook, I. M., Johnson, A., Hatton, P. V., Hill, R. G. and Stanton, K. T., Crystallization modifies osteoconductivity in an apatite-mullite glass-ceramic, J. Mater. Sci: Mater Med. **2003**, 14, 985-990.

Fröberg, L. Hupa, L. And Hupa, M., Porous Bioactive Glasses with Controlled Mechanical Strenght, Key Eng, Mat., **2004**, 254-256, 973-976.

Hench, L.L., Splinter, R. J., Allen, W. C and Greenlee, T. K., Bonding mechanisms at the interface of ceramic prosthetic materials, J. Biomed. Mater. Res., **1971**, 2(1), 117-41.

Hench, L. L. and Paschall, H A., Direct Chemical Bond to Bioactive Glass-Ceramic Materials to Bone and Muscle, J. Biomed. Mater. Res Symp. , **1973**, 4, 25-42.

Hench, L. L. and Paschall, H A., Histochemical responses at a biomaterial's interface, Biomed. Mater. Symposium, **1974**, 5 (1), 49-64.

Hench, L. L., Bioceramics: From Concept to Clinic, J. Am. Ceram. Soc., **1991**, 74(7), 1487-510.

Hench, L. L. and Wilson, J (eds.), An introduction to bioceramics. World Scientific Publishing Co. Pte. Ltd., Singapore, **1993**.

Hench, L. L., The story of Bioglass, J. Mat. Sci. Mat. Med., **2006**, 17(11), 967-978.

Hruby, A., Evaluation of glass forming tendency by means of DTA [differential thermal analysis], J. Phys., **1972**, B22, 1187-1193.

Hupa, L., Karlsson, K. H., Vedel, E., Arstila, H. and Jonson, B., High temperature properties of bioactive glasses, Proceedings of XX A.T.I.V. Conference, Parma Italy, **2005**.

Höland, W. and Beall, G. H., Glass Ceramic Technology, The American Ceramic Society, **2002**, ISBN: 1-57498-107-2.

Ingram, M. D., Mueller, W. and Torge, M., Mixed Alkali Effects in Strong and Fragile Glasses, in The Physics of Non-Crystalline Solids, eds. Pye, D. L., La Course, W. C. and Stevens, H. J., Taylor & Francis Ltd, London, **1992**, ISBN: 0 7484 0050 8.

Itälä, A., Norström, E., Ylänen, H.O., Aro, H, T. and Hupa, M., The Creation of microrough surface in sintered bioactive glass microsperes, J.Biomed. Mater. Res., **2001**, 56(2), 282-8.

Itälä, A., Ylänen, H.O., Yrjans, J. Heino, T., Hentunen, T. Hupa, M. and Aro, H, T., Characterization of microrough bioactive glass surface: Surface reactions and osteoblast responses *in vitro*, J. Biomed. Mat. Res., **2002**, 62(3), 404-411.

Itälä, A., Koort, J., Ylänen, H.O., Hupa, M. and Aro, H, T., Biologic significance of surface microroughening in bone incorporation of porous bioactive glass implants, J. Biomed. Mater.Res. A, **2003**, 67(2), 496-503.

James, P.F., Kinetics of crystal nucleation in silicate glasses, J. Non-Cryst. Solids, **1985**, 73, 517-540.

Jiang, G. Evans, M. E., Jones, I.A., Rudd, C.D., Scotchford, C.A. and Walker, G.S., Preparation of poly(ε-caprolactone)/ continuous bioglass fibre composite using monomer transfer moulding for bone implant, Biomaterials, **2005**a, 26, 2281-8.

Jiang, G. Walker, G.S., Jones, I.A. and Rudd, C.D., XPS identification of surface-initiated polymerization during monomer transfer moulding of poly(ε-caprolactone)/Bioglass® fibre composite, Appl. Surface. Sci., **2005**b, 252, 1854-1862.

Karlsson, K. H. and Rönnlöf, M., Property-composition relationships for potentially bioactive glasses, Glass Sci and Tech, **1998**, 71(5), 141-145.

Karlsson, K. H., Bioactivity of glass and bioactive glasses for bone repair, Glass Technol. **2004**, 45(4), 157-61.

Karlsson, K. H. and Backman, R., in Properties of Glass-Forming Melts, Eds. Pye, L. D. and Montenero, J. I., Taylor & Francis, BocaRaton, **2005**, 11, ISBN:1-57444-662-2.

Kaufmann, E.A., Ducheyne, P., Radin, S., Bonnell, D. A. and Composto, R., Initial events at the bioactive glass surface in contact with protein-containing solutions, J. Biomed. Mater. Res., **2000**, 52(4), 825-830.

Kim, H. M., Miyaji, F., Kokubo, Ohtsuki, C. and Nakamura, T., Bioactivity of Na2O-CaO-SiO2 glasses, J. Am. Ceram. Soc., **1995**, 78, 2405-11.

Kingery, W. D., Introduction to Ceramics, by John Wiley & Sons, Inc, **1960**, 60-53448.

Koga, N., Strnad, Z., Sestak, J. and Strnad, J., Thermodynamics of non-bridging oxygen in silica biocompatible glass-ceramics, Mimetis material for the bone tissue substitution, J. Therm. Anal. Cal., **2003**, 71, 927-937.

Kokubo, T., Sakka, I.S. and Yamamuro, T., Formation of a high-strenght bioactive glass-ceramic in the system MgO-CaO-SiO_2-P_2O_5, J. Mat. Sci., **1986**, 21, 536-540.

Kokubo, T., Kushitani, H., Sakka, S. Kitsugi, T. and Yamamuro, T., Solutions able to reproduce *in vivo* surface-structure changes in bioactive glass-ceramic A-W, J. Biomed. Mater. Res., **1990**, 24, 721-734.

Kokubo, T., Kushitani, H., Ohtsuki, C., Sakka, S. and Yamamuro, T., Chemical reaction of bioactive glass and glass-ceramic with a simulated body fluid, J. Mater. Sci.: Mater. Med., **1992**, 3, 79-83.

Lakatos, T., Johansson, L.-G. and Simmingsköld, B., Kristallisationsegenskaper hos glas i SiO2-Al2O3-Na2O-K2O-CaO- MgO systemet, Glasteknisk Tidskrift, 1974, 29, 43-47.

Lefebvre, L., Chevalier, J., Gremillard, L., Zenati, R., Thollet, G., Bernache-Assolant, D. and Govin, A., Structural transformations of bioactive glass 45S5 with thermal treatments, Acta Mat. **2007**, 55, 3305-3313.

Levin, E.M, Robbins, C.R. and McMuredie H.F., Phase Diagrams for ceramists, The American Ceramic Society, Inc., Ohio, **1964**, 175.

Li, R. Clark, A. E. and Hench, L. L., An investigation of bioactive glass powders by sol-gel processing, J. Appl. Biomat., **1991**, 2(4), 231-9.

Likitvanichkul, S. and LaCourse, W. C., Apatite-wollastonite glass-ceramics, Part I Crystallization kinetics by differential thermal analysis, J. Mat. Sci., **1998**, 33, 5901-5904.

Lockyer, M. W. G., Holland, D. and Dupree, R., NMR investigation of the structure of some bioactive and related glasses, J. Non-Cryst. Solids, **1995**, 207-219.

Maquet, V., Boccaccini, A.R., Pravata, L., Notingher, I. and Jerome, R., Porous poly(α-hydroxyacid)/Bioglass® composite scaffolds for bone tissue engineering. I: preparation and in vitro characterization, Bioamaterials, **2005**, 25, 4185-4194.

Marcolongo, M., Ducheyne, P. and LaCourse, W. C., Surface reaction layer formation in vitro on a bioactive glass fiber/polymeric composite, J. Biomed. Mater. Res., **1997**, 37, 440-8.

Marcolongo, M., Ducheyne, P., Garino, J. and Schepers, E., Bioactive glass fiber/polymeric composites bond to bone tissue, J. Biomed. Mater. Res. **1998**, 39(1), 161-70.

Marotta, A., Buri, A. and Valenti, G. L., Crystallization kinetics of gehlenite glass, J. Mater. Sci., **1978**, 13, 2483-86.

Marotta, A., Saiello, S., Branda, F. and Buri, A., Activation energy for the crystallization of glass from DDTA curves, J. Mater. Sci., **1982**, 17, 105-8.

Matusita, A. & Sakka. S., Kinetis Study on Crystallization of glass by differential thermal analysis – criterion on application of Kissinger plot, J. Non-Cryst. Solids, **1980**, 38-39, 741-6.

Morey, G. W. The Properties of Glass, by Reinhold Publishing Corporation, second ed., **1954**.

Nascimento, M. L. F., Souza, L. A. and Ferreira, E. B., Can glass stability parameters infer glass forming ability?, J. Non-Cryst. Sjolids, **2005**, 351, 3296-3308.

Niemelä, T., Niiranen, H. and Kellomäki, M., Self-reinforced composites of bioabsorbable polymer and bioactive glass with different bioactive glass contensts. Part II: In vitro degradation, Acta Biomat., **2008**, 4, 156-164.

Niiranen, H., Pyhältö, T. Rokkanen, Paatola, T. and Törmälä, P., Bioactive Glass 13-93/P(L/DL)LA Composites in vitro and in vivo, Key Eng. Mater. **2001**, 192-195, 721-724.

Paatola, T., Pirhonen, E., and Törmälä, P., Coating of Bioactive Glass (13-93) Fibers with Bioabsorbable Polymer, Key Eng. Mat., **2001**, 192-195

Pascual, M. J., Duran, A. and Prado, M.O., A new method for determining fixed viscosity points of glasses, Phys. Chem. Glasses, **2005**, 46(5), 512-520-

Paul, A., Chemistry of glasses, by Chapman and Hall Ltd, **1982**, ISBN: 0-421-23020-8.

Pazzaglia, U. E., Gabbi, C., Locardi, B., Di Nucci, A., Zatti, A. and Cherubino, P., Study of the osteoconductive properties of bioactive glass fibers, J. Biomed. Mater. Res. **1989**, 23, 1289-1297.

Peitl, O., Zanotto., E. D. And Hench, L.L., Highly bioactive P_2O_5- Na_2O-CaO-SiO_2 glass-ceramics, J. Non-Cryst. Solids, **2001**, 292, 115-126.

Pelton, A. D. and Wu, P., Thermodynamic modeling in glass-forming melts, J. Non-Cryst. Solids, **1999**, 253, 178-191.

Pirhonen, E. M., Grandi, G. and Törmälä, P., Bioactive glass fiber/polylactide composite, Key Eng. Mat. **2001**, 192-195 (Bioceramics), 725-728.

Prado, M. O., Fredericci, C. and Zanotto, E.D., Glass sintering with concurrent crystallization. Part 2, Phys. Chem. Glasses, **2002**, 43(5), 215-23.

Purola, J. J. Kuidutettavan lasin viskositeettiparametrien määrittäminen, Tampere University of Technology, Department of Mechanical Engineering, Report 15/**1984**.

Pye, L. D., Stevens, H. J. and LaCourse, W. C., Introduction to Glass Science, Plenum Press, New York, USA, **1972**.

Quinteiro, E., Boschi, A.O., Leonelli, C., Manfredini, T. and Siligardi, C., Glass-Ceramic systems compatible with the firing conditions used in the ceramic tile industry, QualiCer, **2002**, 301-311.

Rawlings, R. D., Bioactive Glasses and Glass Ceramics, Clinical Materials, **1993**, 14, 155-179.

Rawlings, R. D. and Boccaccini, A. R., Crystallization and sintering of frits obtained from silicate wastes, Glass Technol., **2004**, 45, 108-111.

Rawson, H., Properties and Applications of Glass, by Elsevier Scientific Publishing Company, **1980**, ISBN: 0-444-41922-5.

Ray, H. S., Measurement of Melting Temperatures of Blast Furnace Slags by Temperature Gradient Melting, Metallurgical Transactions B, **1979**, 10B, 677-9.

Rizkalla, A. S., Jones, D. W., Clarke, D. B. And Hall, G.C., Crystallization of experimental bioactive glass compositions, J. Biomed. Mater. Res. **1996**, 32, 119-124.

Sakka, S. and MacKenzie, J. D., Relation between apparent glass transition temperature and liquidus temperature for inorganic glasses, J. Non-Cryst. Solids, **1971**, 6,145-162.

Schiller, W., Horte, C.-H. and Wiegmann, J., Uber Aussagemöglichkeiten der DTA beim Studium des Kristallisations- und Sinterverhaltens von Gläsern. Wissenschaftliche Beiträge der F. Schiller-Universität, Jena, **1981**, 45-52.

Scholze, H. Influence of viscosity and surface tension on hot-stage microscopy measurements on glasses, Ver. Dtsch. Keram, Ges., **1962**, 391, 63-68.

Shelby, J. E., Introduction to Glass Science and Technology. The Royal Society of Chemistry, Thomas Gramham House, **1997**, ISBN:0-85404-533-3.

Siligardi, C., D'Arrigo, M. C. and Leonelli, C., Sintering Behavior of Glass-Ceramic Frits, Am. Ceram. Soc. Bull., **2000**, 79(8), 88-92.

Stanworth, J. E., Tellurite glasses, J. Soc. Glass Technol., **1952**, 36, 217-41.

Tas, A.C., Synthesis of Biomimetic Ca-Hydroxyapatite Powders at 37°C in Synthetic Body Fluids, Biomat., **2000**, 21, 1429-1438.

Turnbull, D., Undercooling of liquids, Sci. Am., **1965**, 212, 38.

Uhlmann, D. R. and Kreidl, N.J. (eds.), Glass: Science and Technology; v.1, by Academic Press, Inc, **1983**, ISBN: 0-12-706701-9.

Vedel, E., Arstila, H. Ylänen, H, Hupa, L. and Hupa, M., Predicting Physical and Chemical Properties of Bioactive Glasses from Chemical Composition. Part I: Viscosity Characteristics, *accepted* to Glass Technol – Part A.

Vehkamäki, H., Classical Nucleation Theory in Multicomponent Systems, by Springer, **2006**, ISBN: 10 3-540-29213-6.

Vogel, W., Glass Chemistry, Second ed., by Springer-Verlag, **1994**, ISBN: 3-540-57572-3.

Väkiparta, M., Forsback, A.-P., Lassila, L. V., Jokinen, M. Yli-Urpo, A. U. O. and Vallittu, P. K., Biomimetic mineralization of partially bioresorbable glass fiber reinforced composite, J. Mat. Sci: Mater Med., **2005**, 16, 873-879.

Wallenberger, F. T., Melt viscosity and modulus of bulk glasses and fibers: Challenges for the next decade, Glastech. Ber. Glass Sci. Technol. **1997**, 70C, 63-75.

Wallenberger, F. T. and Weston, N. E., Glass Fibers from High and Low Viscosity Melts, Mat. Res. Soc. Symp. Proc. **2002**, 702, 165-172.

Wallenberger, F. T., Hicks, R. J. and Bierhals, A. T., Design of environmentally friendly fiberglass compositions: ternary eutectic SiO_2-Al_2O_3-CaO compositions, structures and properties, J. Non-Cryst. Solids, **2004**, 349, 377-387.

Wakasugi, T., Burgner, L. L. and Weinberg, M. C., A DTA study of crystal nucleation in Na_2O-SiO_2 glasses, J. Non-Cryst. Solids, **1999**, 244, 63-73.

Warren, B. E., Summary work on Atomic Arrangement in Glass, J. Am Ceram. Soc., **1941**, 24(8), 256-61.

Weinberg, M.C., Homogeneous crystal nucleation in glasses, in The Physics of Non-Crystalline Solids, eds. Pye, D. L., La Course, W. C. and Stevens, H. J., Taylor & Francis Ltd, London, **1992**, ISBN: 0 7484 0050 8.

Weinberg, M. C., Poisl, W. H. and Granasy, L., Crystal Growth and classical nucleation theory, C. R. Chimie, **2002**, 5, 765-771.

Wilburn, F. W. and Dawson, J. B., Differential Thermal Analysis 2; Glass, Ed. MacKenzie, R. C., Akademic Press Inc. London, **1972**, ISBN: 0-12-464402-3.

Xu, X. J., Ray, C. S. and Day, D. E., Nucleation and crystallization of $Na_2O{\cdot}2CaO{\cdot}3SiO_2$ glass by differential thermal analysis, J. Am. Ceram. Soc., **1991**, 74(5), 909-14.

Ylänen, H.O., Helminen, T., Helminen, A., Rantakokko, J., Karlsson, K. H. and Aro, H. T., Porous Bioactive Glass Matrix in Reconstruction of Articular Osteochondral Defect, Annales Chirurgiae et Gynaecologiae, **1999**, 88, 237-245.

Ylänen, H.O., Karlsson, K. H. Itälä, A. and Aro, H. T., Effect of immersion in SBF on porous bioactive implants made by sintering bioactive glass microspheres, J. Non-Cryst. Solids, **2000a**, 275, 107-115.

Ylänen, H.O., Helminen, T., Helminen, A., Mattila, K., Karlsson, K. H. and Aro, H. T., Comparison of new bone ingrowth into unloaded porous titanium and bioactive glass implants, 6th World Biomater. Congr. Hawaii, USA, **2000b**.

Ylänen, H.O., Ekholm, C., Beliaev, N., Karlsson, K. H. and Aro, H. T., Comparison of Three Methods in Evaluation of Bone Ingrowth into Porous Bioactive Glass and Titanium Implants, Key Eng. Mat., **2001**, 192-195, 613-616.

Zanotto, E. D., Isothermal and adiabatic nucleation in glass, J. Non-Cryst. Solids, **1987**, 89, 361-70.

Zanotto, E. D., Fokin, V. M., Recent studies of internal and surface nucleation in silicate glasses, Phil. Trans. R. Soc. Lond. A., **2003**, 361, 591-613.

Zanotto, E. D. and Prado, M.O., Isothermal sintering with concurrent crystallization of monodispersed and polydispersed glass particles. Part I. Phys. Chem. Glasses, **2001**, 42(3), 215-23.

Zarzycki, J., Glasses and the vitreous state. 1. Glass. Physical Properties, by Cambridge University Press, **1991**, ISBN: 0 521 35582 6.

Zachariasen, W. H., The atomic arrangement in glass, J. Am. Chem. Soc., **1932**, 54, 10, 3841-51.

Zhang, D., Vedel, E., Hupa, L. Aro, H. T. and Hupa, M., Predicting Physical and Chemical Properties of Bioactive Glasses from Chemical Composition. Part III: Chemical Composition and *In vitro* Reactivity of Glasses, *accepted* to Glass Technol – Part A.

Zhang, D., Vedel, E., Hupa, L. Yländen, H. and Hupa, M., *In vitro* Characterization of Bioactive Glasses, Key Eng. Mater., **2005**, 284-286, 481-484.